Available online at www.sciencedirect.com
ScienceDirect
Coordination Chemistry Reviews 251 (2007) 897–924
COORDINATION CHEMISTRY REVIEWS
www.elsevier.com/locate/ccr

Review

The coordination chemistry of boraamidinate ligands

Chantall Fedorchuk, May Copsey, Tristram Chivers *

Department of Chemistry, University of Calgary, Calgary, Alberta, Canada T2N1N4

Received 21 June 2006; accepted 21 June 2006
Available online 27 June 2006

Contents

* Corresponding author. Tel.: +1 403 220 5741; fax: +1 403 289 9488.
E-mail address: chivers@ucalgary.ca (T. Chivers).

0010-8545/$ – see front matter
doi:10.1016/j.ccr.2006.06.010

Abstract

The boraamidinate ligand, $[RB(NR')_2]^{2-}$, is isoelectronic with the corresponding and extensively studied amidinate ligand, $[RC(NR')_2]^-$. This review provides the first comprehensive account of the coordination chemistry of the boraamidinate ligand with s-, p- and d-block metals. The focus is on the methods available for the synthesis of metal complexes, as well as the variety of bonding modes exhibited by these dianionic ligands at metal centers. The properties and reactivity of individual metal boraamidinates are discussed and, where appropriate, compared with those of the related amidinate complexes. In particular, the formation of the radical anion, $[RB(NR')_2]^{-\bullet}$, by the oxidation of main group complexes is highlighted.

Keywords: Boraamidinates; Coordination complexes; Synthetic methods; Bonding modes; Stable radicals

1. Introduction

Coordination complexes play an essential role in the creation of new materials. Examples of applications range from their role as catalysts for the generation of organic polymers to their incorporation in novel molecular magnets. They are also of increasing interest as single-source precursors of thin film semi-conducting materials or nanoparticles, and in the generation of ceramics. Fundamental investigations into the syntheses and solid-state structures of metal complexes of new or emerging ligand systems are an essential prelude to probing potential future applications.

Extensive studies of amidinate (*am*) ligands, $[RC(NR')_2]^-$, have shown the steric and electronic properties of *ams* are readily varied by changing the organic substituents, R and R′, often affecting the metal coordination geometry. The monoanionic *am* ligands can display a variety of bonding modes. Most commonly, *ams* act as four-electron donors and coordinate in a bidentate fashion through *N*,*N*′ chelation. The coordination chemistry of the *am* ligand up to 1994 is summarized in two reviews, which cover the syntheses and structural features of a comprehensive range of s-, p-, d- and f-block metal complexes [1].

More recently, the focus of investigation into *am* complexes has shifted to their reactivity, in particular their role as polymerization catalysts. These experimental studies have been complimented by detailed theoretical investigations [2]. Early polymerization studies focused on group 4 *am* complexes that were found to be active catalysts for various substrates [3–8]. Vanadium-based *am* complexes have been used in the polymerization of ethylene [9,10]. Copper *am* complexes have been described as air- and moisture-tolerant catalysts for the living polymerization of carbodiimides [11], as well as precursors for atomic layer deposition of copper metal [12]. Yttrium(III) arylamidinates have shown catalytic activity in *rac*-lactide (LA) polymerization [13]. The ring-opening polymerization (ROP) of ε-caprolactone using lanthanide *am* complexes has been reported [14,15]. Research has also focused on *am* complexes containing aluminum as the central element that can also serve as catalysts [16–22].

From this overview it can be inferred that the field of *am* coordination chemistry has reached maturity. By contrast, investigations of the isoelectronic boraamidinate (*bam*) ligand are much more limited [23]. Like the *am* ligand, the electronic and steric properties of the *bam* ligand can be tuned by changing the substituents on the amido nitrogen atoms (R′) and by variation of the R substituent on boron. The three-atom backbone of the *bam* framework is structurally similar to that of the *am* ligand, with replacement of carbon by electron-accepting boron at the bridgehead (Chart 1). Significantly, this substitution generates a 2^- charge on the *bam* ligand. This is in contrast to the monoanionic *am* ligand, which may require additional ancillary anionic ligands in higher oxidation-state metal complexes. The dianionic charge also leads to interesting redox behavior, for example the generation of stable neutral radicals of p-block metal *bam* complexes [24].

The focus of this review is the coordination chemistry of the dianionic boraamidinate (*bam*) ligand $[RB(NR')_2]^{2-}$. The first *bam* metal complex was reported in 1979 [25]. Investigations prior to 1998 were limited to complexes of groups 4 and 14–16 metals [26–38]. More recently, interest in these dianionic ligands has been rekindled through reports of (i) the structural characterization of dilithio *bams* [39–41], (ii) a solid-state study of dithallium complexes [42], (iii) trisubstituted octahedral group 4 dianions (tris-*bams*) [43], (iii) a titanium mono-*bam* used in polymerization studies [44], (iv) a paramagnetic vanadium(IV) *bam* complex [43], (v) *bam* complexes in which the ligand bridges very short group 6 metal–metal triple bonds [45], (vi) spirocyclic zinc and magnesium complexes [46], (vii) group 13 *bam* complexes [41,47], and (viii) paramagnetic early main-group metal *bam* complexes [24,46]. In addition, a new ligand comprised of a five-atom backbone that is a hybrid of the *bam* and *am* skeletons has recently been reported (Chart 2) [41,48]. These hybrid *bamam* ligands are formally isoelectronic with the ubiquitous β-diketiminate (*nacnac*) ligands [49].

This review will begin with an examination of the various methods available for the synthesis of metal complexes of the *bam* ligand. This will be followed by a brief description of the different bonding modes adopted by the *bam* ligand in the solid state. The second half of the review consists of a survey of individual s-, p- and d-block metal complexes. The final section is

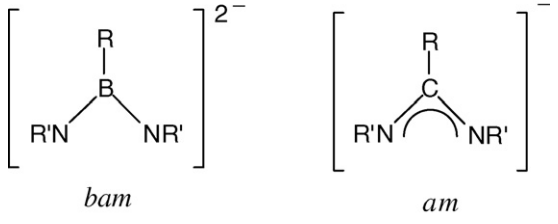

Chart 1.

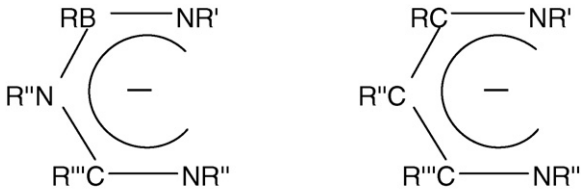

bamam *nacnac*

Chart 2.

devoted to a discussion of the chemistry of the hybrid *bamam* ligands.

2. Synthetic methods

The most common route to *bam* metal complexes employs metathesis between a metal halide and a dilithio *bam* complex, $Li_2[RB(NR')_2]$. Consequently, this section will begin with a discussion of the syntheses of these important boron-containing reagents. Other methods for the syntheses of *bam* complexes include the use of trimethylsilylamido reagents and cycloaddition reactions.

2.1. Metallation of bis(amino)boranes

The metallation of bis(amino)boranes is a potentially useful approach to *bam* complexes of alkali and alkaline earth metals. The preparation of dilithiated reagents **2** (Scheme 1) represents the widest use of this approach. Bis(alkylamino)phenylboranes $PhB[N(H)R']_2$ (**1**) have been known since 1957 [50]. A variety of derivatives have been prepared by the reaction of $PhBCl_2$ with four equivalents of the appropriate amine [51]. More recently, compound **1** (R = Ph) has been prepared from the reaction of dichlorophenylborane with four equivalents of a lithiated alkylamide [40a] as shown in Scheme 1. The monoamino derivatives (**3**) are prepared from the reaction of dichlorophenylborane with two equivalents of a primary amine (Scheme 1) [41]. Asymmetrically substituted bis(amino)phenylboranes (**4**) are obtained by treatment of the monoamino chloroborane $PhBCl[N(H)R']$ with an excess of a lithium amide.

The first dilithio *bams* $Li_2[RB(NR')_2]$ (**2**) were reported in 1990. They were prepared by dilithiation of $PhB[N(H)R']_2$ with ^{n}BuLi and used as *in situ* reagents in reactions with metal halides [27,28]. More recently, an alternative and potentially more versatile route to B-alkyl or B-aryl *bams* was reported that involves the reaction of tri(alkylamino)boranes $B[N(H)R']_3$ (**5**) with three equivalents of an organolithium reagent RLi (R = alkyl, aryl) (Scheme 2) [39]. In addition to effecting dilithiation, the RLi reagents serve as nucleophiles, replacing one N(H)R′ group by the substituent R. This method allows for variation of the substituent on boron, by the use of different RLi reagents, and avoids the need to prepare dichloroboranes $RBCl_2$. The application of this method led to the first X-ray structural characterization of a dilithio *bam* complex [39,40a].

In 2002, it was shown that the reaction of trisaminoboranes **5** with three equivalents of an organolithium reagent can also lead to the formation of trilithiated imidoboranes [52,53]. The latter can exist as the trilithio complex, as in the case of the anilido derivative **6**, which dimerizes in the solid-state incorporating molecules of lithium chloride. However, when the organic substituent on nitrogen is 2-pyridyl, the observed product is $Li_4[B(NR)_3NHR](THF)_3$ (**7**). This complex consists of the fully deprotonated $[B(NR)_3]^{3-}$ trianion and a molecule of Li[N(H)R]. This suggests that both triple deprotonation and B–N bond cleavage occur in this reaction. The steric and electronic shielding of the boron atom, as well as the solvent used, has also been shown to have an effect on the reaction pathway. When using this method as a synthetic route to dilithiated boraamidinate complexes, the competition between deprotonation and formation of the borate, as well as B–N bond cleavage must be considered. The coordination chemistry of the $[B(NR)_3]^{3-}$ trianion with a wider range of metals has yet to be investigated.

The widely used reagent $Li_2[RB(NR')_2]$ (**2**, R = Ph, R′ = ^{t}Bu) can be prepared by either of the two aforementioned methods. However, the preferred synthesis is the dilithiation of $PhB[N(H)^tBu]_2$, since this method avoids the need to separate the product, by crystallization, from $Li[N(H)^tBu]$.

Examples of metallation reactions involving organomagnesium or organoaluminum reagents are limited to one for each metal. The bis-solvated magnesium *bam*

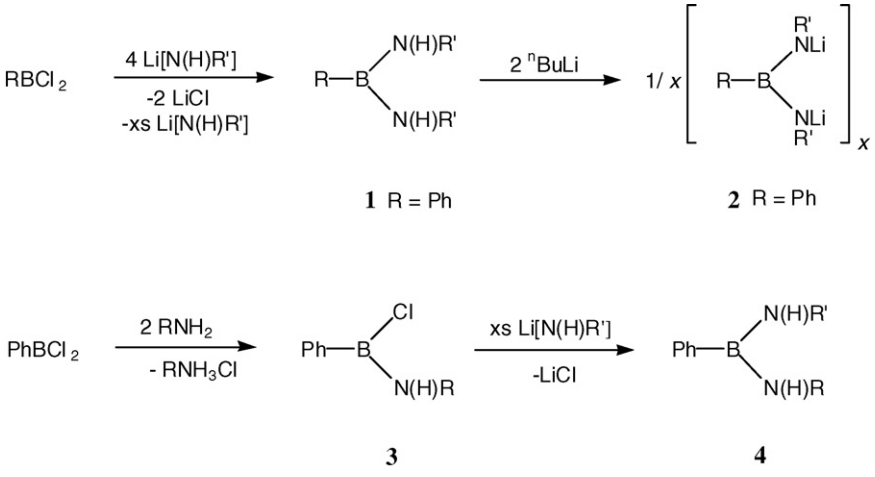

Scheme 1.

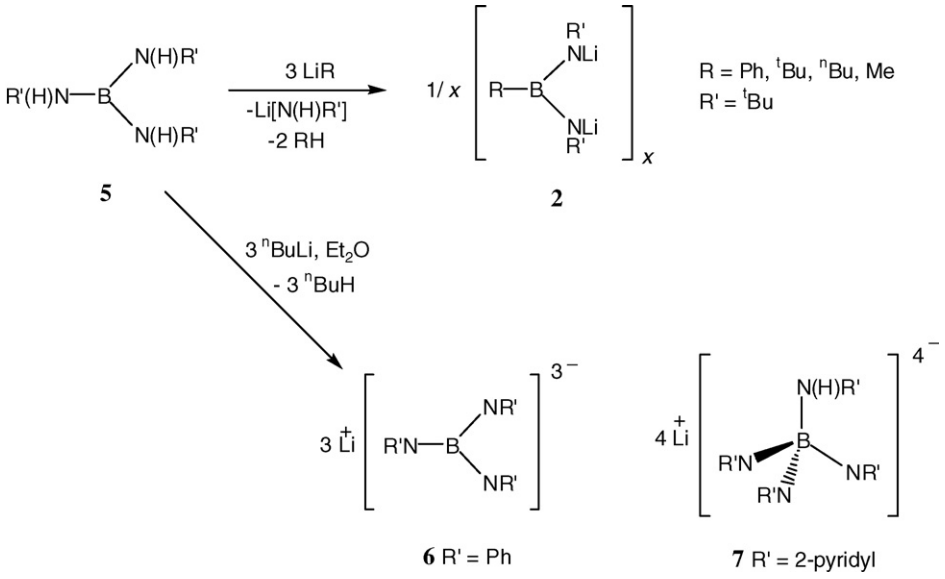

Scheme 2.

complex $Mg(OEt_2)_2[PhB(\mu\text{-}NDipp)_2]$ (**8**) (Dipp = 2,6-di-*iso*-propylphenyl) is obtained by the reaction of the bis(amino)borane **1** (R = Ph, R′ = Dipp) with an excess of $^{n/s}Bu_2Mg$ (Scheme 3) [47].

Methane elimination occurs in the reaction of $Mes^*B(NHMe)_2$ (Mes^* = 2,4,6-($^tBu)_3C_6H_2$) with trimethylaluminum in hot toluene to give the aluminum *bam* complex $[Mes^*BN(Me)Al(Me)N(Me)–]_2$, which was assigned an eight-membered ring structure on the basis of the observation of a molecular ion for the dimer in the EI mass spectrum [35].

2.2. Metathesis using dilithio complexes

A selection of the main-group metal *bam* complexes that have been produced by the reaction of dilithio *bam* reagents with the appropriate metal halide is shown in Chart 3. This metathetical approach has provided mono- and bis-*bam* complexes of the following s- and p-block elements: Mg (**9**) [47], Al (**10**, **13**), Ga (**11**, **14**, **16**, **18**), In (**12**, **15**, **19**) [24,41,46,47], Tl (**17**) [42], Ge (**20**), Sn (**21**) [27,32,38], Te (**22**, **23**) [34,40], Pb (**24**) [27,28,38], P (**25**) [40a], As (**26**), Sb (**27**) and Bi (**28**) [40b].

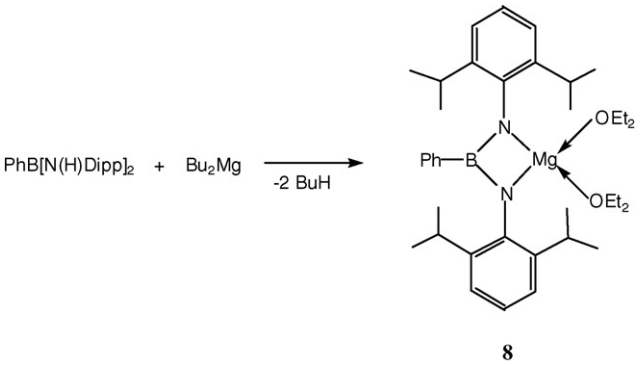

8

Scheme 3.

The reactions of dilithio *bams* with organometallic halide reagents have been shown to generate the expected organometallic *bam* complexes. The treatment of $Li_2[PhB(N^tBu)_2]$ with a Grignard reagent in a 1:2 stoichiometry affords the di(organomagnesium)*bam* complexes **29** and **30** in 37–66% yields (Scheme 4) [46].

The heterometallic complex $Mg[PhB(\mu_3\text{-}N^tBu)_2]_2(LiOEt_2)_2$ (**9**) can be prepared by metathesis of two equivalents of $Li_2[PhB(N^tBu)_2]$ with $MgCl_2$ [46]. More unusually, this same compound is also obtained in excellent yield by the reaction of $Li_2[PhB(N^tBu)_2]$ with a variety of Grignard reagents in a 1:1 stoichiometry (Scheme 4) [46].

The reactions of $Li_2[RB(NR')_2]$ with dimethyltin dihalides produces either mono or bridging organotin *bam* complexes (**31** and **32**), which have been isolated with a variety of different substituents on the boron and nitrogen atoms in 30–70% yields (Scheme 5) [27,32,38].

The transition-metal *bam* complexes that have been obtained by the metathetical approach are illustrated in Chart 4. The list includes mono-, bis- or tris-*bam* complexes of Ti (**33**, **35**), Zr (**34**, **36**, **38**), Hf (**37**, **39**) [27,43,44], V (**42**) [43], Zn (**43**) [46a] and Cd (**44**) [46b], as well as Mo (**40**), W (**41**) complexes in which the *bam* ligand bridges two transition-metal centers [45]. In common with main-group metal *bam* complexes, $Li_2[PhB(N^tBu)_2]$ has served as the most common dilithio reagent for transferring the *bam* ligand to transition-metal centers via metathesis.

2.3. Reactions of dichloroboranes with dilithiobis(amino) reagents

Examples of the reaction of dichloroboranes with dilithiated bis(amino) reagents are restricted to the formation of a tellurium *bam* complex $[PhB(\mu\text{-}N^tBu)_2]Te(=N^tBu)$ (**45**) from dichlorophenylborane with $\{Li_2[Te(N^tBu)_3]\}_2$ (Scheme 6) [36]. The latter reagent may be considered as the dilithiated derivative of the bis(amino)iminotellurane $[^tBuN(H)]_2Te=N^tBu$. In view of the extensive variety of dilithiated bis(amino) reagents avail-

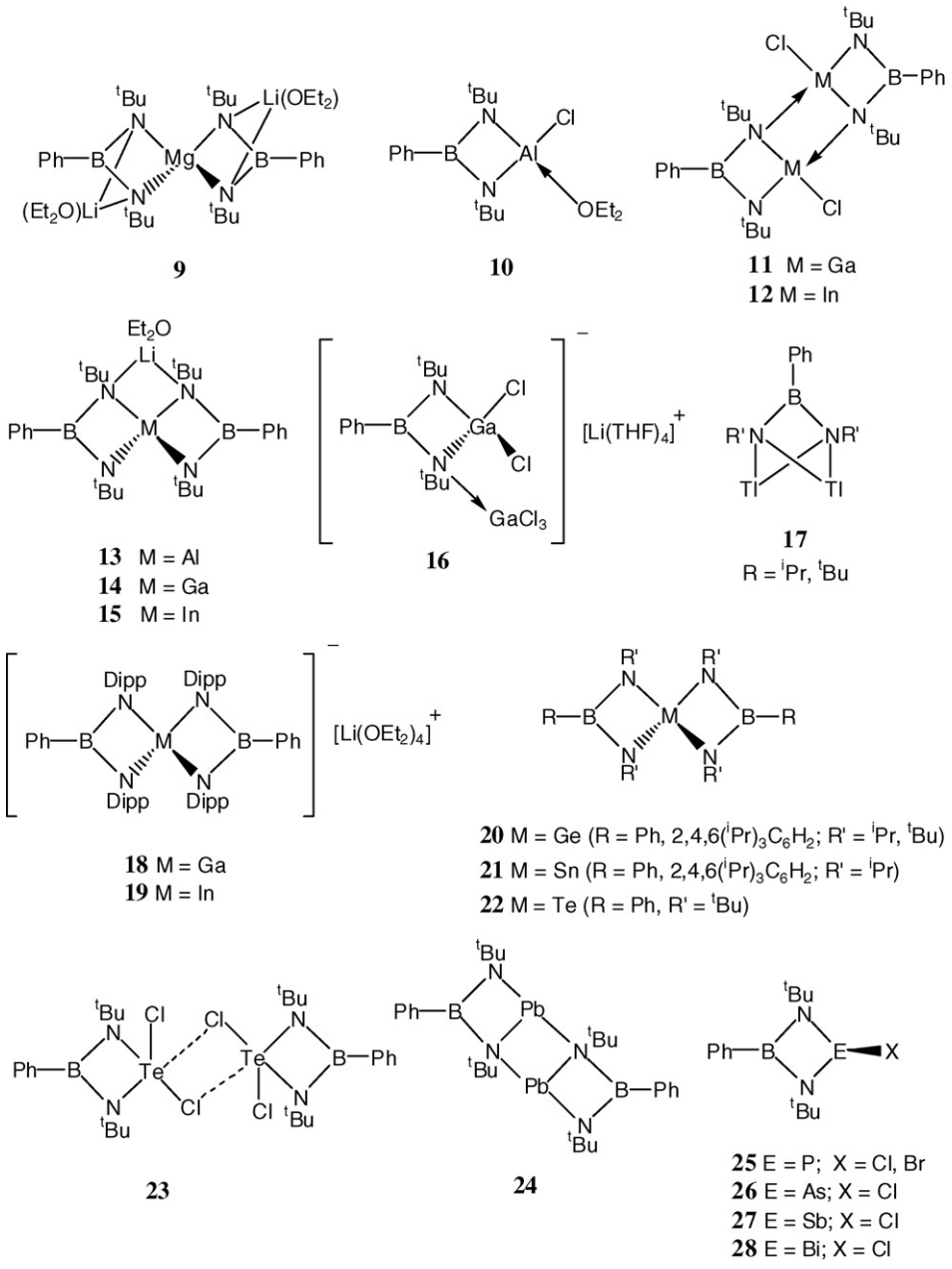

Chart 3.

able for main group elements [54,55], this synthetic method is potentially of wide application.

2.4. Cycloaddition reactions

A variety of cycloaddition reactions have produced silicon, phosphorus, and sulfur mono-*bam* complexes. For example, the photolytically generated silylene: $SiMes_2$ reacts with the iminoborane $[(Me_3Si)^tBuN]B{=}N^tBu$ to generate the silicon complex $[MesB(\mu\text{-}N^tBu)_2]Si(Mes)(SiMe_3)$ (**46**) in 23% yield (Scheme 7) [31].

The initial product **47** of the cycloaddition of *tert*-butyl(*tert*-butylimino)borane with *tert*-butyl(*tert*-butylimino)phosphane undergoes disproportionation to give two phosphorus-containing products. The *bam* complex $[^tBuB(\mu\text{-}N^tBu)_2]P^tBu(=N^tBu)$ (**49**) contains a phosphorus(V) atom, while the other product (**48**) combines with a further equivalent of $^tBuP{=}N^tBu$ to produce the P–P bonded species $[^tBuB(\mu\text{-}N^tBu)_2]^tBuP\text{–}P^tBu$ (**50**) (Scheme 8) [26].

Reactions of *N*,*N*′-substituted sulfur diimides with alkyl or aryl bis(methylthio)boranes proceeds via a 1,3-cycloaddition with the formation of sulfur(II) *bam* complexes (**51**) in 38–85% yield (Scheme 9). This reaction presumably involves the reductive elimination of MeS–SMe [29,30].

2.5. Use of trimethylsilylamido reagents

In a few cases, the reaction of trimethylsilylamido reagents with metal chlorides has been employed to produce *bam* complexes using the formation of trimethylsilyl chloride as

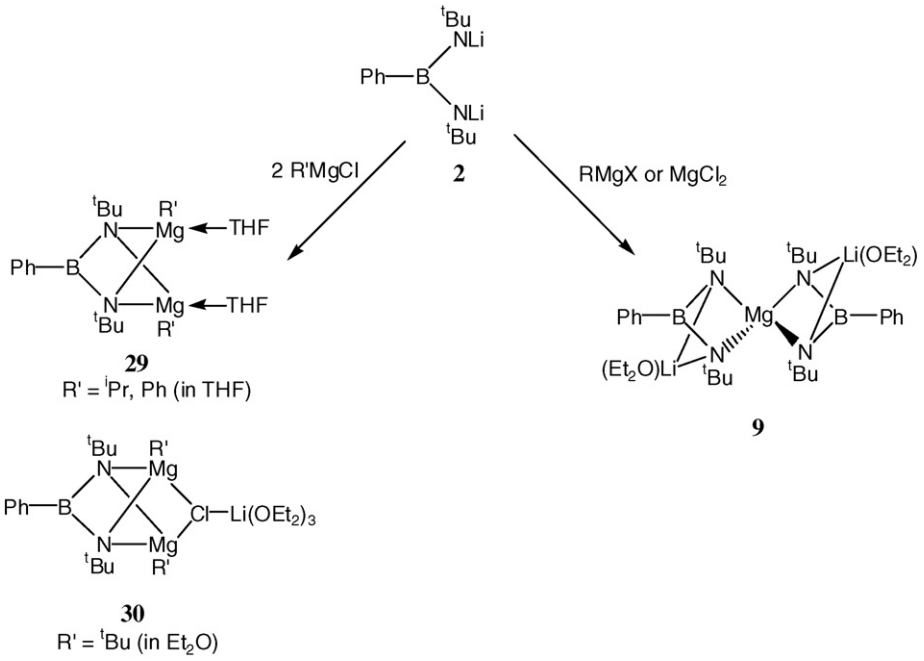

Scheme 4.

the driving force. An intriguing example is the reaction of $MeN[PhB(NMeSiMe_3)]_2$, which embraces an NBNBN framework, with titanium tetrachloride to give the binuclear titanium *bam* complex $Ti_2(\mu\text{-}NMe)Cl_4[PhB(\mu_3\text{-}NMe)_2]$ (**52**) and the borazine $[Ph_3B_3N_3Me_3]$ (**53**) (Scheme 10) [33]. The formation of **53** formally results from the elimination, and subsequent trimerization, of the "PhBNMe" monomer during the course of the reaction.

2.6. Miscellaneous methods

The fluoro-bis(amino)borane $FB[N(H)Dipp][N(SiMe_3)R]$ ($R = {}^t Bu$) (**54**) reacts with ^{t}BuLi in a 1:1 molar ratio, with elimination of LiF, to give the iminoborane **55**, which isomerizes to form the silicon *bam* complexes $Me_2Si[MeB(\mu\text{-}NDipp)(\mu\text{-}N{}^t Bu)]$ (**56**) and $Me_2Si[MeB(\mu\text{-}NDipp)_2]$ (**57**) in 20 and 54% yields, respectively (Scheme 11) [37]. When this reaction is carried out in a 1:2 molar ratio, *tert*-butyl *bam* derivatives $Me_2Si[{}^t BuB(\mu\text{-}NDipp)(\mu\text{-}NR)]$ (**58**) are produced in 63–74% yields (Scheme 11). These silicon derivatives contain rare examples of unsymmetrical *bam* ligands, i.e. with different substituents on the two nitrogen atoms.

The reaction of $Li[N(BMe_2)(SiMe_3)]$ with $SnCl_2$ results in a low yield (6.5%) of the dimeric complex $\{Sn[MeB(\mu\text{-}NSiMe_3)_2]\}_2$ (**59**). This process is thought to involve an initial metathesis followed by ring closure with the elimination of BMe_3 (Scheme 12) [25].

3. Bonding modes

The primary emphasis of the investigations into *bam* complexes synthesized up to this time has been on structural characterization in the solid state. The diversity of bonding modes observed is outlined schematically in Chart 5. For the sake of clarity, the substituents R and R′ on the boron and nitrogen atoms of the *bam* ligand are omitted.

3.1. Mono-boraamidinate

3.1.1. Bonding mode *A*

Bonding mode **A** involves *N*,*N*′-chelation of a single *bam* ligand to a single metal center (Chart 5). It is the most common coordination motif for *bam* complexes. In general, the B–N bond distances in the *bam* ligands in complexes of this type are

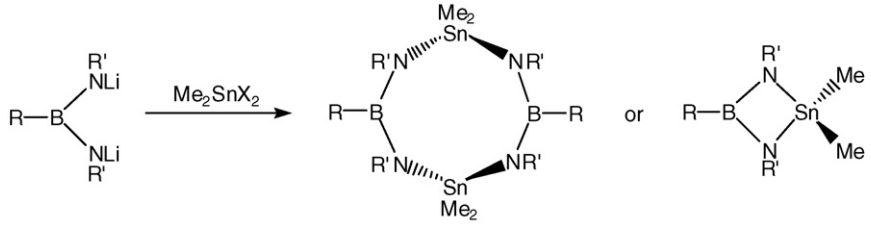

Scheme 5.

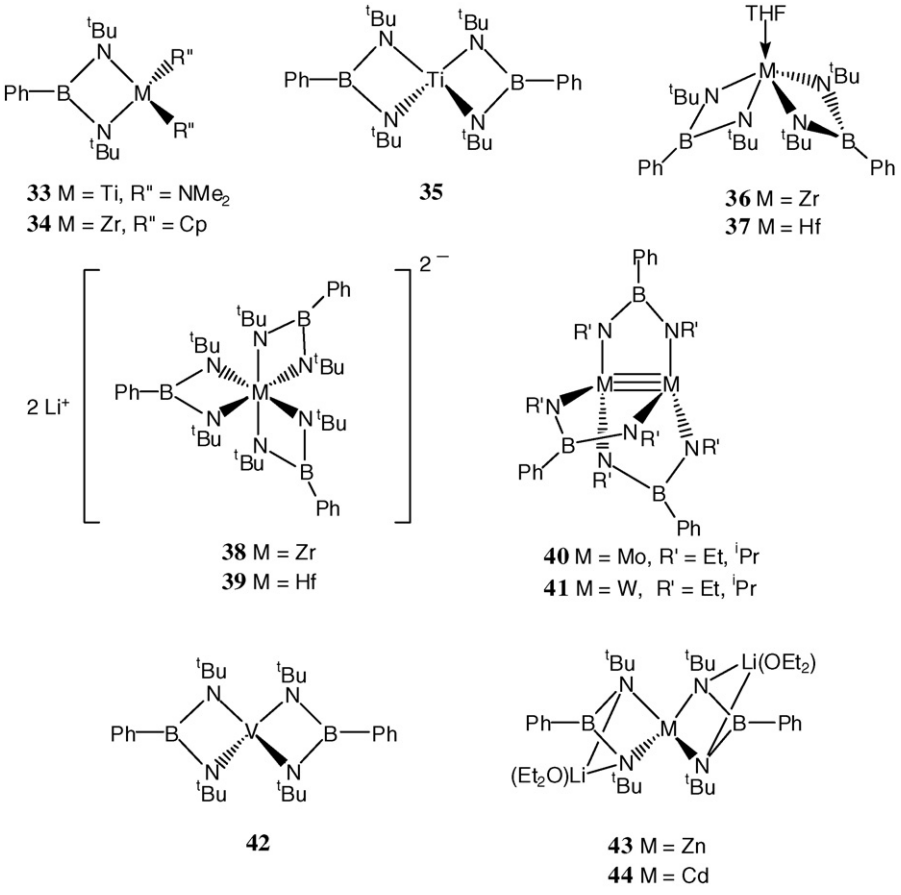

Chart 4.

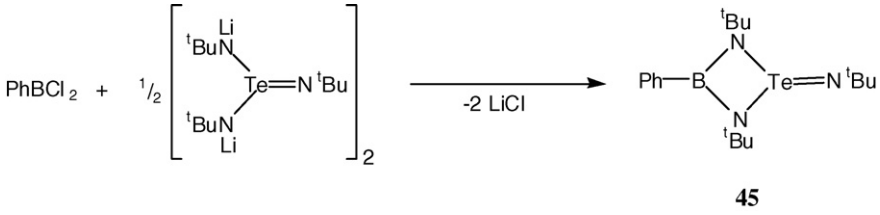

Scheme 6.

equal within experimental error and fall within the narrow range of 1.436(2)–1.471(4) Å reflecting delocalized boron–nitrogen bonding. The N–B–N bond angles fall within the range 102.6(4)–112.5(3)°. In most cases the four-membered MNBN ring is essentially planar.

3.1.2. Bonding mode *B*

Bonding mode **B** is found in dimeric complexes in which monomeric units (mode **A**) are connected by additional M–N bonds (Chart 5). Thus the *bam* ligands in these complexes exhibit one three-coordinate and one four-coordinate N atom. As expected, there are significant differences between the two B–N bond lengths in the *bam* ligands of these complexes, as well as disparity between M–N bond distances, resulting from the different coordination environments of the nitrogen atoms. The M–N bond lengths linking the two monomer units are not much longer than those observed in the MNBN metallacycles for all complexes.

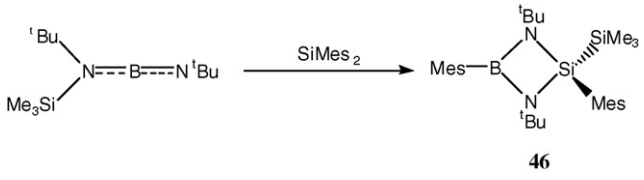

Scheme 7.

3.2. Bis-boraamidinate

3.2.1. Bonding mode *C*

In bonding mode **C**, two *bam* ligands *N*,*N*′-chelate the central metal or element in a spirocyclic fashion (Chart 5). This is the second most common mode observed for *bam* complexes characterized by X-ray crystallography thus far. With the exception

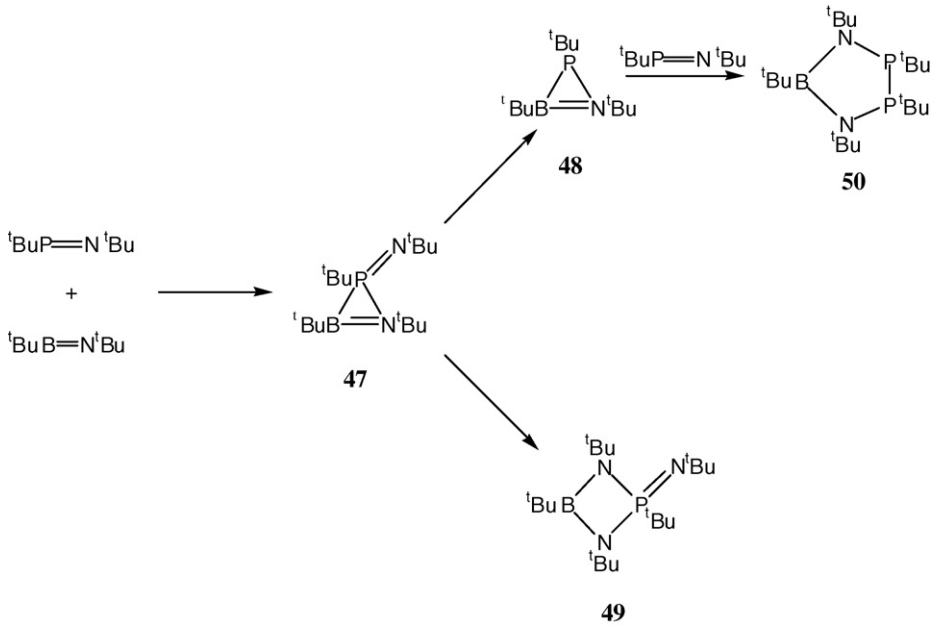

Scheme 8.

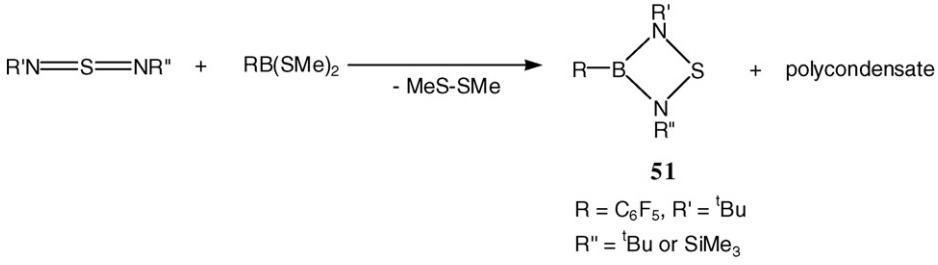

Scheme 9.

of the di-*iso*-propylphenyl derivatives **18** and **19** [41] (Chart 3), all of the bis-*bam* complexes displaying mode **C** contain the $[PhB(N^tBu)_2]^{2-}$ ligand. The spirocyclic neutral radicals $\{[PhB(\mu\text{-}N^tBu)_2]_2M\}^{\bullet}$, formed by one-electron oxidation of the corresponding anions, have also been structurally characterized in the solid state and these show that the *bam* ligand retains bonding mode **C** when oxidized [24].

Three examples of neutral spirocycles of the type $M[PhB(\mu\text{-}N^tBu)_2]_2$, M = Ti (**35**) [27], M = V (**42**) [43], and M = Te (**22**) [34], have been reported. The B–N bond distances in these complexes fall in the range 1.411(7)–1.48(1) Å, very similar to bonding mode **A**, while the mean M–N distances and NMN angles reflect the increasing atomic size of the central atom (Table 1).

3.3. Tris-boraamidinates

3.3.1. Bonding mode *D*

Bonding mode **D** applies to complexes in which three *bam* ligands *N*,*N*′-chelate a single pseudo-octahedral metal center. Examples of tris-*bam* complexes reported to date are confined to complexes of larger transition metals. The group 4 complexes $Li_2[M\{PhB(\mu_3\text{-}N^tBu)_2\}_3]$ M = Zr (**38**), M = Hf (**39**) adopt this bonding mode [43].

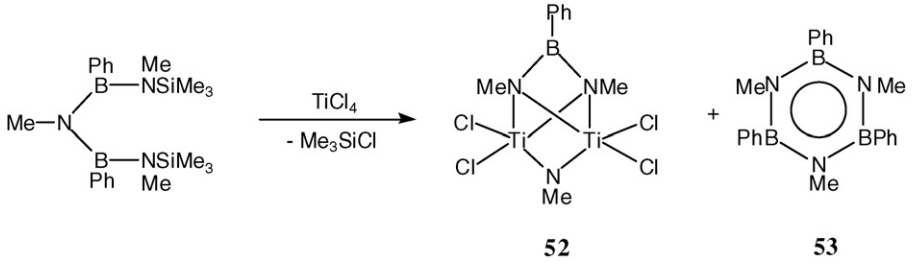

Scheme 10.

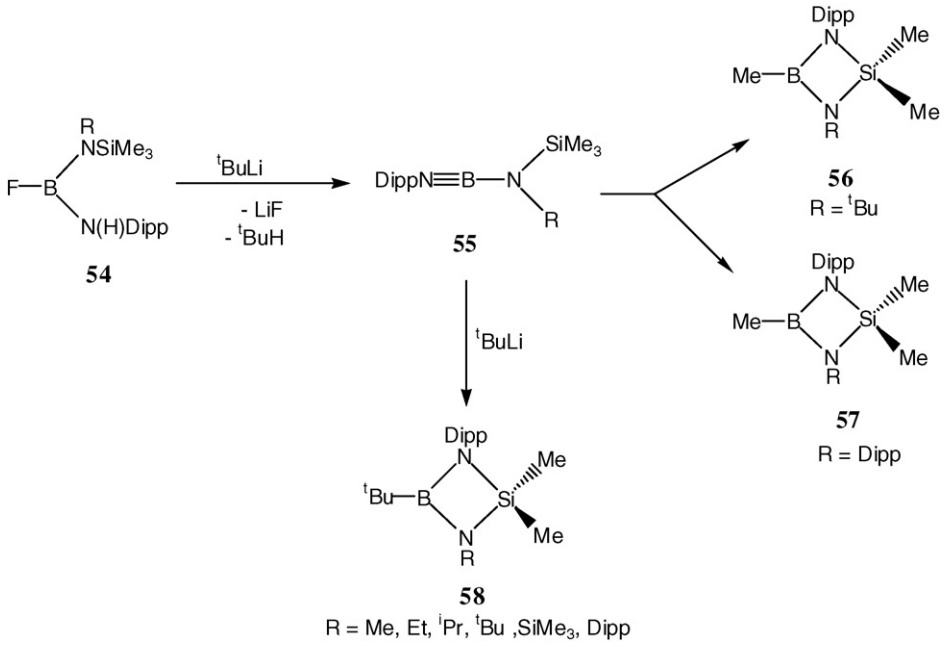

Scheme 11.

3.4. Bridging boraamidinates

3.4.1. Bonding mode *E*

The third most common bonding mode found in *bam* complexes is that in which both nitrogen atoms of the *bam* ligand bridge two metal centers (Chart 5). The widely used dilithium reagents $Li_2[RB(NR')_2]$ (**2**) [39,40a] and the thallium(I) complexes $Tl_2[PhB(\mu_3\text{-}NR')_2]$ (**17**) (R′ = ^{i}Pr, ^{t}Bu) exhibit bonding mode **E** [42].

The magnesium complex $(^t BuMg)_2[PhB(\mu_3\text{-}N^tBu)_2]\cdot LiCl(OEt_2)_3$ (**30**) (Scheme 4) and the titanium complex $Ti_2[PhB(\mu_3\text{-}NMe)_2](\mu\text{-}NMe)Cl_4(THF)_2$ (**52**) (Scheme 10) also adopt bonding mode **E** [33,46]. In **30**, both nitrogen atoms of the *bam* ligand are linked to two magnesium centers which, in turn, are bridged by the chloride ion of a LiCl molecule [46]. Similarly each nitrogen atom of the *bam* ligand in **52** connects two titanium centers, which are bridged by an NMe group [33]. In both complexes, the B–N bond distances are equal within experimental error with a mean value of *ca.* 1.45 Å. The Mg atoms in **30** adopt very distorted tetrahedral geometries (bond angle range *ca.* 66–138.5°) with the smallest angles associated with the N–Mg–N unit, while the Ti atoms in **52** are in a distorted octahedral environment.

3.4.2. Bonding mode *F*

In bonding mode **F**, two *bam* ligands bridge two metal centers to give an eight-membered ring (Chart 5). It can be considered as an alternative to mode **B** for the dimerization of two four-

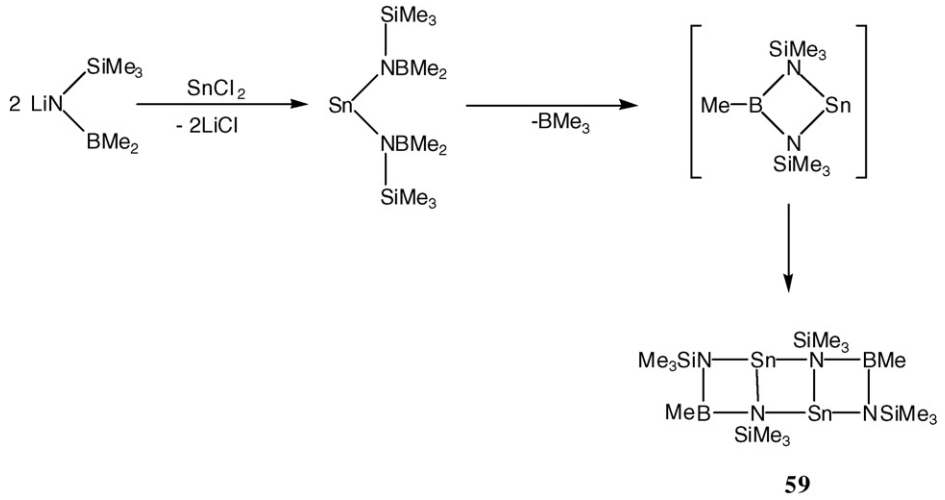

Scheme 12.

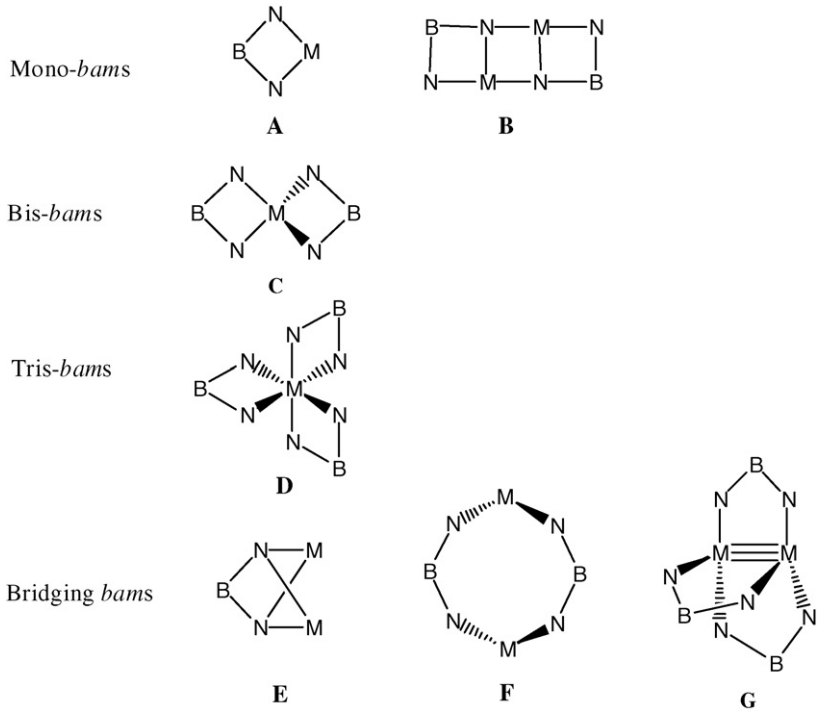

Chart 5.

membered rings. In the case of **F**, however, ring-opening occurs to give an eight-membered ring with only three-coordinate nitrogen atoms. This is one of the less common coordination motifs for *bam* complexes and only two examples have been reported. The tin complexes $\{SnMe_2[\mu\text{-}RB(NMe)_2\kappa^2N,N']\}_2$ (**31**, R = 2,4,6-(^{i}Pr)$_3$C$_6$H$_2$ or Mes*) (Scheme 5) [38,35] exhibit an $Sn_2N_4B_2$ ring in a chair conformation. Although the Sn–N bond lengths are similar to those found for the mono-*bam* tin complex **32** $[C_6F_5B(\mu\text{-}N^tBu)_2]SnMe_2$ (*ca.* 2.06 Å) [32], the N–B–N and N–Sn–N bond angles are significantly larger than those observed for group 14 *bam* complexes involving four-membered SnNBN rings.

3.4.3. Bonding mode *G*

Bonding mode **G** involves three *bam* ligands spanning a metal–metal triple bond (Chart 5), an arrangement that has only been observed for the group 6 complexes **40** and **41**, M≡M[μ-PhB(NR′)$_2\kappa^2N,N']_3$ (M = Mo, W), which exhibit pseudo-D_{3h} symmetry [45].

4. A survey of boraamidinate complexes

In this section individual *bam* complexes will be surveyed with an emphasis on their syntheses and solid-state structures. Important structural parameters for all complexes that have been characterized by single crystal X-ray crystallography are summarized in Table 1. The discussion is divided into sub-sections that, in sequence, discuss *bam* complexes of s-, p- and d-block elements. The formation of complexes containing a [*bam*] radical anion coordinated to the metal center is a recurring feature of the chemistry of early main-group systems.

4.1. s-Block metal complexes

Groups 1 and 2 *bam* complexes have been limited to lithium and magnesium derivatives. An area of possible future study is the generation of heavier alkali-metal complexes that may serve as alternative reagents for the transfer of the *bam* ligand to other metal centres.

4.1.1. Lithium

The first X-ray structural determinations of dilithio *bam* complexes were reported in 2000 [39–41]. Those investigations showed that the extent of aggregation is influenced by the organic substituent (R) on both boron and nitrogen. The fundamental building block is the Li_2N_2B unit [39,40] (Chart 6). In the case of the dimers $\{Li_2[RB(\mu_3\text{-}N^tBu)_2]\}_2$, R = Ph (**60**), ^{n}Bu (**61**), ^{t}Bu (**62**), two of these units participate in a face-to-face interaction through lithium–nitrogen contacts to give a bicapped cube. In the trimeric example $\{Li_2[MeB(\mu_3\text{-}N^tBu)_2]\}_3$ (**65**), three Li_2N_2B units associate edge-on through lithium–nitrogen contacts to give a tricapped hexagonal prism [39]. This demonstrates that a small change in the substituent at the boron bridgehead may affect the size of the aggregate formed in the solid state. It is noted, however, that the multinuclear (^{1}H, ^{11}B, and ^{7}Li) NMR spectra of the crude product, prior to recrystallization of **65**, reveals the presence of a second oligomer tentatively identified as the dimer $\{Li_2[MeB(\mu_3\text{-}N^tBu)_2]\}_2$ (**63**) [39].

Small changes in the size of the imido substituents can also have an effect on the extent of aggregation in the solid state. For example, the *iso*-propyl derivative $\{Li_2[PhB(\mu_3\text{-}N^iPr)_2]\}_3$ (**66**) is trimeric [42], whereas the *tert*-butyl analogue **60** is dimeric.

Table 1
Selected bond distances (Å) and bond angles (°) for *bam* complexes

Compound	Bonding mode	B–N	M–N	N–B–N	N–M–N
PhB[N(H)Dipp]$_2$ [41]		1.420(3), 1.414(3)		118.5(2)	
Group 1					
{Li$_2$[PhB(μ$_3$-N^{t}Bu)$_2$]}$_2$ [40a]	**E**	1.448(3), 1.449(3)	2.017(4)–2.077(4)	109.5(2)	69.9(1)–110.6(2)
{Li$_2$[^{n}BuB(μ$_3$-N^{t}Bu)$_2$]}$_2$ [39]	**E**	1.451(4)–1.464(4)	2.009(6)–2.091(5)	108.2(2), 108.5(2)	71.0(2)–110.8(2)
{Li$_2$[^{t}BuB(μ$_3$-N^{t}Bu)$_2$]}$_2$ [40a]	**E**	1.476(4), 1.479(4), 1.476(2)	1.976(4)–2.154(5)	105.2(2), 105.5(2)	72.0(2)–113.2(2)
{Li$_2$[MeB(μ$_3$-N^{t}Bu)$_2$]}$_3$ [39]	**E**	1.451(3)–1.456(3)	2.001(4)–2.100(4)	110.0(2), 110.5(2)	70.8(1)–153.7(2)
Li$_2$(THF)$_2$(μ-THF)[PhB(μ$_3$-NDipp)$_2$] [41]	**E**	1.415(5), 1.446(4)	2.010(6)–2.115(6)	111.4(3)	71.8(2), 69.1(2)
Li$_2$(Et$_2$O)$_2$[PhB(μ$_3$-NDipp)(μ$_3$-N^{t}Bu)] [41]	**E**	1.428(3), 1.451(3)	1.985(5), 2.010(4)	109.9(2)	72.3(2), 72.5(2)
{Li$_2$[PhB(μ$_3$-N^{i}Pr)$_2$]}$_2$ [42]	**E**	1.437(2)–1.439(2)	1.995(7)–2.117(7)	112.0(2), 112.9(2)	70.8(3), 70.9(2)
{Li$_2$[PhB(μ$_3$-N(2-OMe)C$_6$H$_4$)$_2$]}$_2$ [56]	**E**	1.430(2), 1.429(2)	1.984(3)–2.090(3)	116.8(1)	105.1(1), 107.5(1)
Group 2					
Mg(Et$_2$O)$_2$[PhB(μ-NDipp)$_2$] [46a]	**A**	1.439(5), 1.449(5)	1.985(3), 1.973(3)	112.5(3)	74.7(1)
{Li(Et$_2$O)]Mg[PhB(μ$_3$-N^{t}Bu)$_2$]}$_2$ [46a]	**C**	1.446(2)–1.449(2)	M = Mg: 2.086(1)–2.093(1); M = Li: 2.023(3)–2.045(3)	106.7(1), 107.1(1)	M = Mg: 67.54(5)–138.54(5); M = Li: 69.88(9), 69.56(9)
(^{t}BuMg)$_2$[PhB(μ$_3$-N^{t}Bu)$_2$]·LiCl(OEt$_2$)$_3$ [46[46a]	**E**	1.446(3), 1.456(3)	2.131(2)–2.192(2)	105.6(2)	65.53(8), 65.73(8)
Group 4					
Ti[PhB(μ-N^{t}Bu$_2$)]$_2$ [27]	**C**	1.48(1), 1.453(9)	1.880(5), 1.895(5)	110.5(6)	79.2(2)–126.8(3)
[PhB(μ$_3$-NMe)$_2$]Ti$_2$(μ-NMe)Cl$_4$(THF)$_2$ [33]	**E**	1.453(6), 1.447(5)	1.863(3)–2.135(3)		
{[PhBμ-N^{t}Bu)$_2$]Ti(μ-Cl)$_2$}$_n$ [44]	**A**	1.471(4), 1.464(4)	1.852(2), 1.850(2)	109.5(2)	80.7(1)
Bn$_2$Ti[PhB(μ-N^{t}Bu)$_2$] [44]	**A**	1.467(3), 1.455(3)	1.853(2), 1.858(2)	109.3(2)	79.97(8)
Zr(THF)[PhB(μ-N^{t}Bu)$_2$]$_2$ [43]	**C**	1.467(7)	2.122(4), 2.044(4)	111.2(4)	70.5(2)–174.1(2)
Li$_2$Zr[PhB(μ-N^{t}Bu)$_2$][PhB(μ$_3$-N^{t}Bu)$_2$]$_2$ [43]	**D**	1.442(5)–1.480(5)	2.053(3)–2.604(3)	110.4(3), 111.6(3), 109.7(3)	71.9(1), 109.1(1), 58.5(1)
Li$_2$Hf[PhB(μ-N^{t}Bu)$_2$][PhB(μ$_3$-N^{t}Bu)$_2$]$_2$ [43]	**D**	1.42(1)–1.47(1)	2.031(6)–2.752(6)	110.9(8), 112.3(7), 107.8(7)	71.8(2), 59.2(2), 56.1(2)
Hf(THF)[PhB(μ-N^{t}Bu)$_2$]$_2$ [43]	**C**	1.464(9)	2.103(5), 2.030(5)	111.2(4)	71.0(2)–173.5(2)
Group 5					
V[PhB(μ-N^{t}Bu)$_2$]$_2$ [43]	**C**	1.460(5), 1.459(6), 1.459(6)	1.853(3), 1.851(3)	106.9(4)	78.5(1–127.7(2)
Group 6					
Mo≡Mo[μ-PhB(NEt)$_2$κ^2*N*,*N*′)$_3$ [45]	**G**	1.429(7)–1.452(7)	1.975(4)–2.002(4)	117.0(3), 117.9(5), 117.3(5)	
W≡W[μ-PhB(N^{i}Pr)$_2$κ^2*N*,*N*′]$_3$ [45]	**G**	1.44(1)–1.47(1)	1.984(7), 1.985(7), 1.959(8)	118.0(8), 119(1)	
Group 12					
{Li(Et$_2$O)[PhB(μ-N^{t}Bu)(μ$_3$-N^{t}Bu)]}$_2$Zn [46a]	**C**	1.425(7)–1.443(7)	M = Zn: 2.013(4)–2.076(4); M = Li: 2.01(1)–2.07(1)	106.0(5), 106.9(4)	M = Zn: 68.4(2)–136.6(2); M = Li: 69.3(4), 68.4(3)
{Li(Et$_2$O)[PhB(μ-N^{t}Bu)(μ$_3$-N^{t}Bu)]}$_2$Cd[46b]	**C**	1.440(6)–1.448(7)	M = Cd: 2.257(4)–2.272(3); M = Li: 1.993(9)–2.029(9)	107.9(4), 108.2(4)	M = Cd: 62.0(1), 62.2(1); M = Li: 71.0(3), 71.1(3)
Group 13					
[PhB(μ-N^{t}Bu)$_2$]AlCl(OEt$_2$) [47]	**A**	1.442(2), 1.455(2)	1.806(1), 1.802(1)	106.36(9)	79.99(4)
{[PhB(μ-N^{t}Bu)$_2$]$_2$Al}$^\bullet$[24]	**C**	1.445(3), 1.449(3)	1.842(2), 1.852(2)	104.2(2)	76.37(9)–128.5(1)
{[PhB(μ-N^{t}Bu)(μ$_3$-N^{t}Bu]GaCl}$_2$ [47]	**B**	1.552(3), 1.394(3)	1.897(2), 1.966(2), 2.042(2)	107.4(2)	118.73(8), 74.11(8), 89.92(7)
Li(THF)$_4$[PhB(μ-N^{t}Bu)$_2$]GaCl$_2$·GaCl$_3$ [47]	**A**	1.565(4), 1.377(4)	1.880(2), 2.048(2), 1.966(2)	107.2(2)	74.13(9)

Table 1 (*Continued*)

Compound	Bonding mode	B–N	M–N	N–B–N	N–M–N
$Li(Et_2O)Ga[PhB(\mu\text{-}N^tBu)(\mu_3\text{-}N^tBu)]_2$ [47]	**C**	1.491(5), 1.423(5)	1.887(3), 1.974(3)	107.7(4)	75.1(1)–140.9(2)
$\{[PhB\mu\text{-}N^tBu)_2]_2Ga\}^\bullet$ [24]	**C**	1.445(3), 1.438(3)	1.923(2), 1.922(2)	104.7(2)	72.81(9)–130.6(1)
$\{[PhB(\mu\text{-}N^tBu)(\mu_3\text{-}N'Bu)]InCl_2\cdot LiCl(THF)_2$ [47]	**B**	1.393(5)–1.538(5)	2.099(3)–2.566(3)	110.2(3), 112.2(3)	61.2(1)–124.01(2)
$Li(OEt_2)In[PhB(\mu\text{-}N^tBu)(\mu_3\text{-}N^tBu)]_2$ [47]	**C**	1.472(3), 1.424(4)	2.195(2), 2.069(2)	111.6(2)	68.28(8)–157.5(1)
$[Li(OEt_2)_4]\{In[PhB(\mu\text{-}NDipp)_2]_2\}$ [41]	**C**	1.427(6)–1.442(6)	2.123(4)–2.133(3)	110.3(4), 110.8(4)	67.1(1)–143.3(1)
$Tl_2[PhB(\mu_3\text{-}N^tBu)_2]$ [42]	**E**	1.44(4), 1.43(4)	2.40(2)–2.53(3)	109(3)	55.7(8), 58.0(8)
$Tl_2[PhB(\mu_3\text{-}N^iPr)_2]$ [42]	**E**	1.43(2)–1.62(2)	2.38(1)–2.70(1)	119(1), 109(1)	57.4(4)–66.4(5)
Group 14					
$(Mes)(Me_3Si)Si[MesB(\mu\text{-}N^tBu)_2]$ [31]	**A**	1.450(5), 1.436(6)	1.745(4), 1.768(3)	101.6(4)	79.1(1)
$Me_2Si[MeB(\mu\text{-}NDipp)_2]$ [37]	**A**	1.445(2)	1.744(1)	102.5(2)	80.5(1)
$Me_2Sn[C_6F_5B(\mu\text{-}N^tBu)_2]$ [32]	**A**	1.425(9), 1.418(9)	2.050(5), 2.069(5)	109.4(6)	68.6(2)
$\{Me_2Sn[\mu\text{-}2,4,6\text{-}(^iPr)_3C_6H_2B(NMe)_2\kappa^2N,N']\}_2$ [38]	**F**	1.437(3), 1.417(3)	2.059(2), 2.054(2)	117.7(2)	110.51(8)
$\{Me_2Sn[\mu\text{-}Mes^*B(NMe)_2\kappa^2N,N']\}_2$ [35]	**F**	1.425(6), 1.431(6)	2.043(3), 2.066(3)	120.0(4)	113.5(13)
$\{Sn[MeB(\mu\text{-}N\ SiMe_3)(\mu_3\text{-}NSiMe_3)]\}_2$ [25]	**B**	1.48(3), 1.42(2)	2.25(1), 2.23(1), 2.11(1)	112(2)	82.3(5), 67.0(5), 95.0(5)
$Li(THF)LiPb[PhB(\mu_3\text{-}N^tBu)_2]_2$ [46b]	**E**[a]	1.412(4)–1.490(4)	2.309(2), 2.346(3)	106.5(3), 112.9(3)	M = Pb: 59.84(9), 99.47(9), 105.17(9)
$\{Pb[PhB(\mu\text{-}N^tBu)(\mu_3\text{-}N^tBu)]\}_2$ [28]	**B**	1.498(8), 1.39(1)	2.329(6), 2.250(5), 2.407(5)	111.2(5)	62.8(2), 83.8(2), 98.2(2)
Group 15					
$[PhB(\mu\text{-}N^tBu)_2]PBr$ [40a]	**A**	1.440(4)	1.688(3)	97.9(3)	80.1(2)
$[^tBuB(\mu\text{-}N^tBu)_2]P^tBu(=N^tBu)$ [26]	**A**	1.458(3), 1.448(3)	1.709(2), 1.711(2)	98.0(2)	79.7(1)
$[PhB(\mu\text{-}N^tBu)_2]P[N(H)^tBu]$ [40a]	**A**	1.438(2), 1.436(2)	1.740(1), 1.745(1)	98.6(1)	77.37(7)
$\{[PhB(\mu_3\text{-}N^tBu)(\mu\text{-}N^tBu)]P(\mu_3\text{-}N^tBu)Li\}_2$ [40a]	**A**	1.417(2), 1.476(2)	1.766(1), 1.811(1)	99.1(1)	75.99(5)
$LiAs[PhB(\mu\text{-}N^tBu)(\mu_3\text{-}N^tBu)]_2$ [40][40b]	**B**	1.412(4), 1.459(4)	M = As: 1.789(4), 1.968(5), 1.972(5)	109.0(3)	M = As: 76.7(2), 101.3(2), 107.9(2)
$Li(OEt_2)As[PhB(\mu\text{-}N^tBu)_2]_2$ [40b]	**B**[b]	1.371(3), 1.527(2)	M = As: 1.845(2), 1.876(2), 1.962(2)	103.3(2), 116.6(2)	M = As: 72.45(6), 109.38(7), 111.05(7)
$LiSb[PhB(\mu\text{-}N^tBu)(\mu_3\text{-}N^tBu)]_2$ [40b]	**B**	1.411(7), 1.453(8)	M = Sb: 1.938(5), 2.147(5), 2.199(6)	110.5(5)	M = Sb: 69.0(2), 98.5(2), 104.0(2)
$\{Sb[PhB(\mu\text{-}N^tBu)_2]\}_2[\mu\text{-}PhB(N^tBu)_2]$ [40b]	**A**,**F**[c]	1.438(4)–1.463(4)	2.065(3)–2.089(2)	105.7(3), 106.4(3), 116.8(3)	67.9(3), 67.3(1), 103.6(1)–110.3(1)
$Li(OEt_2)Bi[PhB(\mu_3\text{-}N^tBu)_2][PhB(\mu\text{-}N^tBu)(\mu_3\text{-}N^tBu)]$ [40b]	**A**[d]	1.398(5)–1.485(5)	M = Bi: 2.239(3)–2.444(3)	108.5(3), 111.7(3)	M = Bi: 59.6(1), 63.2(1), 91.2(1), 91.6(1), 101.9(1)
Group 16					
$S[PhB(\mu\text{-}N^tBu)_2]$ [30]	**A**	1.439(2)	1.735(1)	98.5(2)	77.8(1)
$S[C_6F_5B(\mu\text{-}N^tBu)_2]$ [29]	**A**	1.417(4)	1.730(3)	99.8(3)	77.6(2)
$\{Cl(\mu\text{-}Cl)Te[PhB(\mu\text{-}N^tBu)_2]\}_2$ [40a]	**A**	1.447(3), 1.447(3)	2.000(2), 2.000(2)	103.5(2)	69.33(7)–97.38(5)
$(^tBuN=)Te[PhB(\mu\text{-}N^tBu)_2]$ [36]	**A**	1.45(1), 1.46(1)	2.081(7), 2.081(6)	104.1(8)	67.0(3)
$Te[PhB(\mu\text{-}N^tBu)_2]_2$ [34]	**C**	1.448(5), 1.411(7), 1.414(8), 1.448(5)	2.147(3), 2.147(3), 2.035(4), 2.037(4)	106.8(4), 106.9(4)	66.5(1), 101.1(1), 161.2(1), 102.1(1), 105.8(2), 66.6(1)

[a] See description in Section 4.2.2.

[b] With loss of transannular Li–N and As–N bonds (see Section 4.2.3).

[c] The third boraamidinate ligand bridges two Sb centres.

[d] See description in Section 4.2.3.

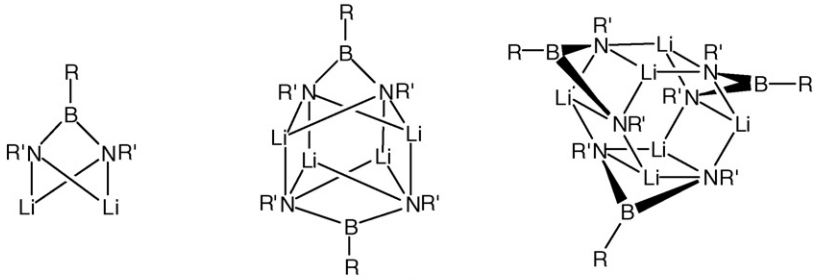

60 R = Ph, R' = ^{t}Bu
61 R = ^{n}Bu, R' = ^{t}Bu
62 R = ^{t}Bu, R' = ^{t}Bu
63 R = Me, R' = ^{t}Bu
64 R = Ph, R' = (2-OMe)C_6H_4

65 R = Me, R' = ^{t}Bu
66 R = Ph, R' = ^{i}Pr

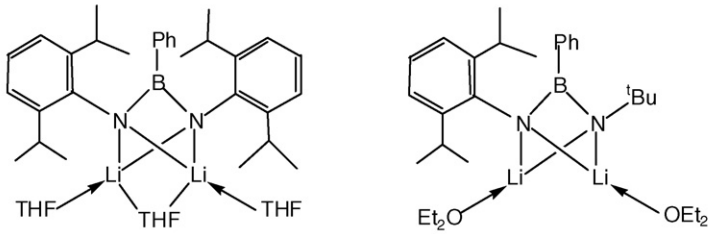

67 **68**

Chart 6.

A dimer is also observed for the case of $\{Li_2[PhB(\mu_3\text{-}N(2\text{-}OMe)C_6H_4)_2]\}_2$ (**64**) where the organic substituent on the imido group features a methoxy side-arm which leads to donation of the oxygen lone pair to the lithium centers [56]. A larger increase in the steric bulk of the substituent at nitrogen leads to the formation of the monomeric dilithio *bams* $Li_2(THF)_3[PhB(\mu_3\text{-}NDipp)_2]$ (**67**) and $Li_2(Et_2O)_2[PhB(\mu_3\text{-}NDipp)(\mu_3\text{-}N^{t}Bu)]$ (**68**) [41], although solvation of the lithium ions may preempt the association via Li–N interactions in these two derivatives.

As indicated in Table 1, the shortest B–N bond distance, 1.415(5) Å, for the dilithio *bams* is observed for the *N*-di-*iso*-propylphenyl derivative **67** [41]. The range of N–B–N bond angles exhibited by these complexes is 105.2(2)–111.4(3)°. The largest value is found in **67** in order to accommodate the steric bulk of the R′ substituents [41]. Agostic C(H)···Li interactions occur in the solid-state structures of the dimeric dilithio *bams* **60–62** and also in the trimeric complex **66**.

In the ^{1}H NMR spectrum (295 K) of **68**, two separate methine resonances and four doublets for the *iso*-propyl methyl groups for the Dipp substituents are observed [41]. These NMR data are unique for *bam* complexes incorporating Dipp substituents, reflecting both the lower symmetry of this molecule and hindered rotation of the *N*-aryl groups in solution. For comparison, the ^{1}H NMR spectra of complexes such as $Me_2Si[MeB(\mu\text{-}NDipp)(\mu\text{-}NR')]$, R′ = ^{t}Bu (**56**), Dipp (**57**), exhibit one septet for the two equivalent methine protons and a pair of doublets of equal intensity for the diastereotopically inequivalent *iso*-propyl methyl groups (Scheme 11) [37]. In contrast, only one resonance is observed in the ^{1}H NMR spectra for both the CH and CH_3 groups of the Dipp substituents of the aminoboranes $PhB[N(H)Dipp]_2$ [41] and $FB[N(H)Dipp][NSiMe_3(R)]$ (**54**) (R = Dipp, ^{t}Bu, Me, Et, ^{i}Pr, $SiMe_3$) [37].

The most significant difference between the behavior of *bam* complexes, compared to that of their *am* counterparts, involves their redox properties. As a result of the 2^{-} charge on the *bam* ligand, it is possible to generate, by a one-electron oxidation, the anionic radical $[bam]^{-\bullet}$ which can be stabilized by coordination to a metal center. The first indications of the formation of paramagnetic early main-group metal *bam* complexes came from investigations of dimeric dilithium derivatives **60–64** in 2002 [40]. It was observed that the initially colorless solutions of these reagents became red upon exposure to air. In preliminary EPR studies, a five-line pattern was resolved, indicating coupling of the unpaired electron to two equivalent ^{14}N nuclei. In subsequent studies, variable-temperature EPR spectroscopic studies revealed the formation of the monocyclic radical $\{[PhB(\mu\text{-}N^{t}Bu)_2]Li(OEt_2)_x\}^{\bullet}$ (**69**) in which the radical monoanion $[PhB(N^{t}Bu)_2]^{-\bullet}$ is chelated to a diethyl ether-solvated lithium cation (Scheme 13) [46]. The experimental EPR spectrum was

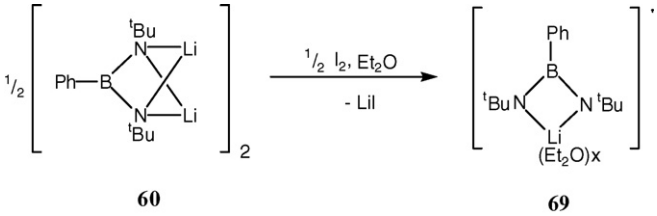

60 **69**

Scheme 13.

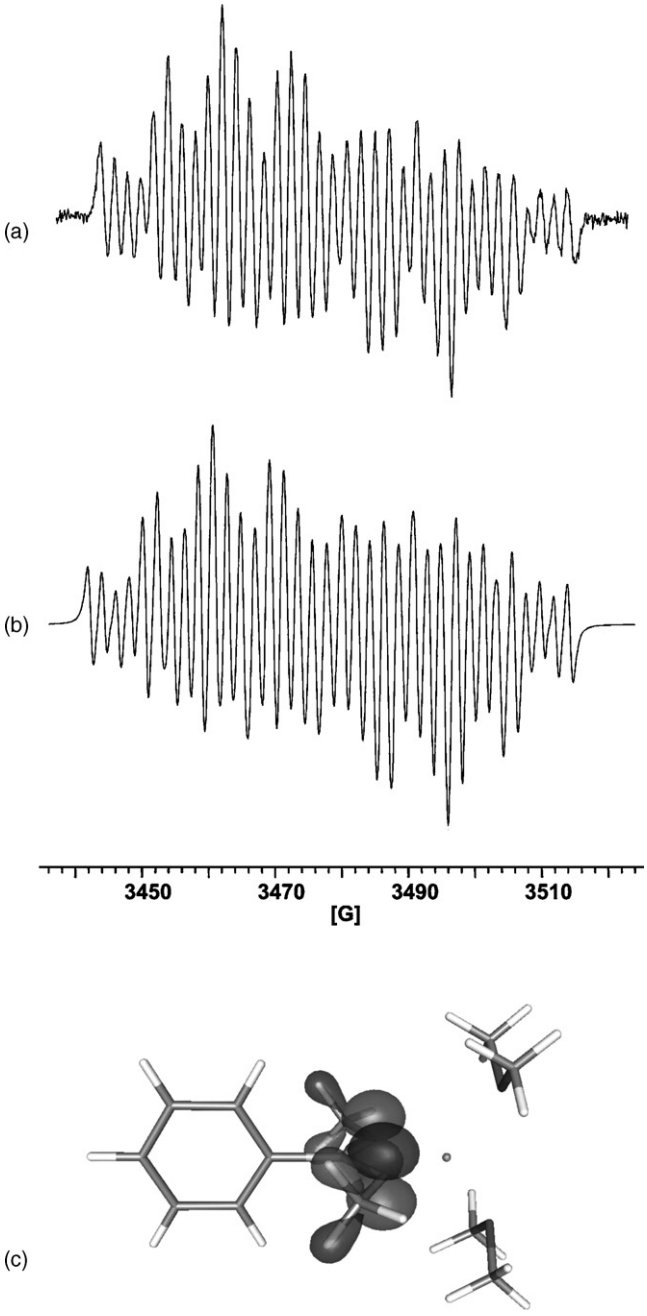

Fig. 1. Experimental (a) and simulated (b) X-band EPR spectra of a diethyl ether solution of $\{[PhB(\mu\text{-}N^tBu)_2]Li(OEt_2)_x\}^\bullet$ (**69**) at 233 K; (c) SOMO (isosurface values ±0.06) of $\{[PhB(\mu\text{-}NMe)_2]Li(OMe_2)_2\}^\bullet$. Reproduced with permission from [46a]. Copyright 2006 American Chemical Society.

simulated by invoking hyperfine interactions of the unpaired electron with *one* lithium atom (^{7}Li, $I = 3/2$, 92.41%; ^{6}Li, $I = 1$, 7.59%), two equivalent nitrogen centers (^{14}N, $I = 1$, 99.6%), and one boron atom (^{10}B, $I = 3$, 19.9%; ^{11}B, $I = 3/2$, 80.1%)] (Fig. 1). The plausibility of this assignment was supported by DFT calculations for the model system $\{[PhB(NMe)_2]Li(OEt_2)_x\}^\bullet$. As indicated in Fig. 1, the electron density in the SOMO of this radical is primarily located on the two nitrogen atoms.

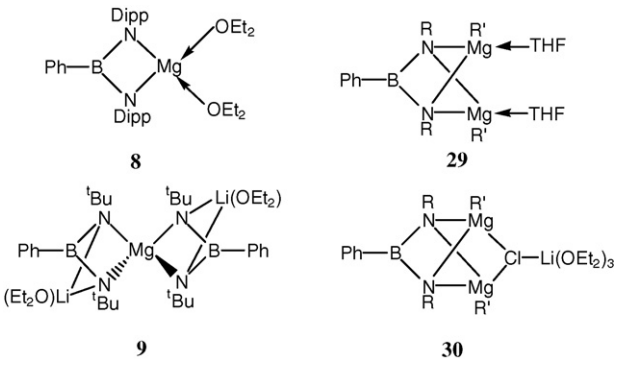

Chart 7.

4.1.2. Magnesium

The chemistry of magnesium complexes of the *am* ligand is extensive [57–60]. They have been used as reagents for the synthesis of transition-metal complexes and as precursors in chemical vapor deposition experiments. By contrast, investigations into magnesium *bam* complexes have been limited to structural determinations and redox behavior.

There are four known structurally characterized examples of magnesium complexes of the *bam* ligand (Chart 7). Complex **8** adopts bonding mode **A** and is formed by the simple double deprotonation of the parent bis(alkylamino)phenylborane using dibutylmagnesium (Scheme 3) [46]. Dimerization of this complex in the solid state is presumably prevented by the bulky di-*iso*-propylphenyl substituents on nitrogen. Instead, the remaining coordination sites on the tetrahedral magnesium center are occupied by two molecules of diethyl ether. Complexes **9**, **29** and **30** are synthesized by metathesis of the appropriate dilithio boraamidinate with Grignard reagents, in varying stoichiometries, as outlined in Section 2.2 (Scheme 4) [46]. Complexes **29** and **30** both adopt bonding mode **D**, with the boraamidinate ligand bridging both metal centres. Complex **30** additionally binds a molecule of the by-product lithium chloride in the solid state, when crystallized from diethyl ether.

The remaining complex **9** assumes bonding mode **C**, involving the *N*,*N*′-chelation of the spirocyclic dianion $\{Mg[PhB(\mu\text{-}N^tBu)_2]_2\}^{2-}$ to two monosolvated lithium cations. The central magnesium atom exhibits a distorted tetrahedral geometry linking two four-membered NBNMg rings that are non-planar. The additional coordination of the nitrogen centers to lithium has no measurable effect on the B–N bond distances, which are the same within experimental error as those observed in complex **8**. The geometry about the nitrogen atoms, however, is quite distorted from ideal tetrahedral angles (ranges: *ca.* 77–135°) with the smallest values associated with the B–N–Li angle.

The stoichiometric oxidation of **9** with iodine has been probed by EPR spectroscopy (Scheme 14) [46]. The experimental EPR spectra, supported by results from DFT calculations, confirm that the resulting bright pink radical $\{Li(Et_2O)Mg[PhB(\mu\text{-}N^tBu)_2][PhB(\mu_3\text{-}N^tBu)_2]\}^\bullet$ (**70**) adopts a C_s-symmetric structure in solution with localized spin density on the *bam* ligand that is *not* coordinated to lithium. The EPR spectrum exhibits hyperfine structure resulting from interaction of the unpaired

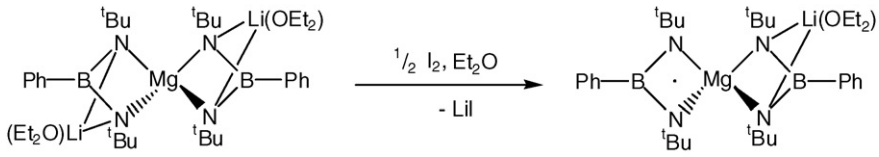

9 70

Scheme 14.

electron with two inequivalent nitrogen atoms, the central metal (^{25}Mg, $I = 5/2$, 10.1%), and one boron atom.

4.2. p-Block metal complexes

Complexes of the p-block elements with *bam* ligands have been studied more extensively than those of s- or d-block metals. Complexes of all group 13–16 elements, with the exception of selenium, are known.

4.2.1. Boron, aluminum, gallium, indium and thallium

The coordination chemistry of the *am* ligand with group 13 elements has been thoroughly investigated [1,16–22,60–69]. This intensive interest has largely been kindled by the observation of the catalytic activity of aluminum *ams* [16–22,63,64]. Group 13 complexes of nitrogen-centered ligands have also attracted recent attention as precursors for electronic materials such as aluminum and gallium nitride [65]. For the related *bam* ligands, the coordination chemistry with group 13 elements has recently been expanded; thirteen complexes, which adopt three of the six observed bonding modes, have been structurally characterized (Table 1). To date, however, no studies of polymerization activity of group 13 *bam* complexes have been reported.

As noted in Section 2.2, the spirocyclic anions $\{M[PhB(N^tBu)_2]_2\}^-$, M = Al (**13**), Ga (**14**), In (**15**), as their lithium derivatives are prepared by metathesis of two equivalents of $Li_2[PhB(N^tBu)_2]$ with the appropriate metal halide (Scheme 15). These anions are *N*,*N*′-chelated to a monosolvated lithium cation when R = ^{t}Bu (**13**–**15**) [47], whereas a solvent-separated ion pair is formed for the bulkier Dipp derivatives (**18** and **19**), which are prepared in a similar manner [41].

A perusal of the structural parameters listed in Table 1 reveals that the bond angles at the central group 13 element deviate markedly from tetrahedral (ranges *ca*. 75–141° in 14; 68–157.5° in **15**). This distortion is partly due to the *N*,*N*′-chelation of the anion to a monosolvated lithium counter-ion. The B–N bond distances involving three-coordinate nitrogen in the four-membered BN_2M rings are *ca*. 0.05 Å shorter than those involving four-coordinate nitrogen atoms. Concomitantly, there are significant differences of *ca*. 0.1 Å in the M–N distances

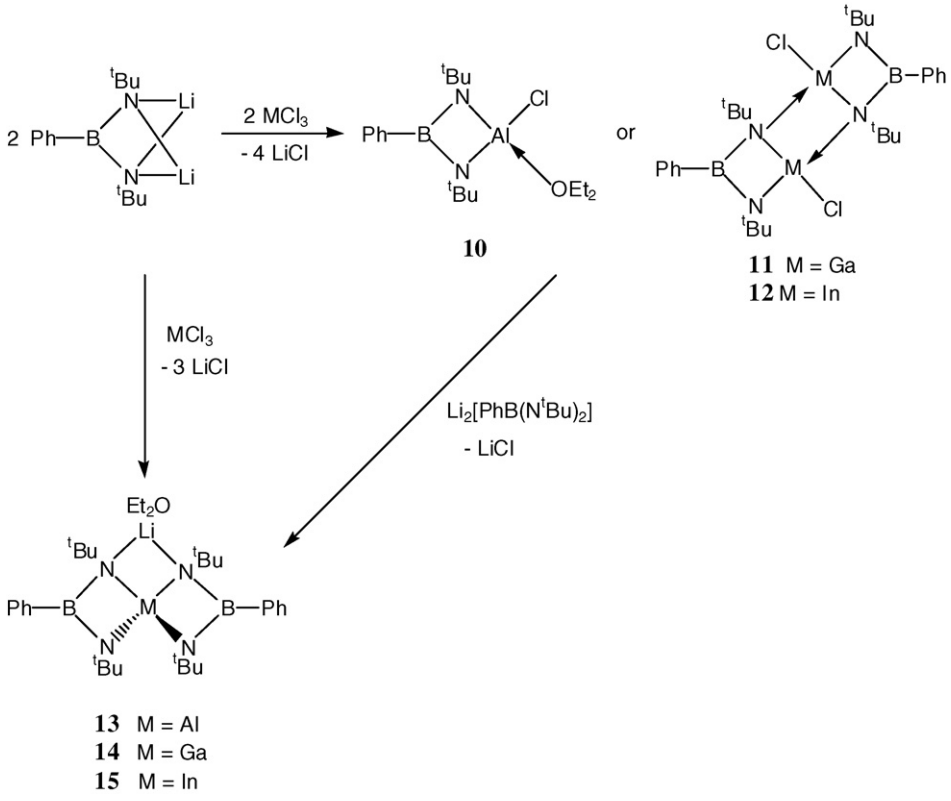

10

11 M = Ga
12 M = In

13 M = Al
14 M = Ga
15 M = In

Scheme 15.

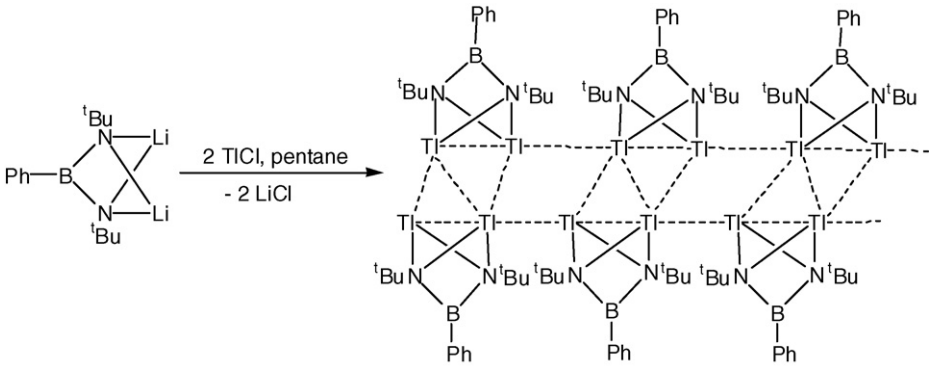

17

Scheme 16.

involving the three- and four-coordinate nitrogen atoms. In contrast, all the nitrogen atoms are three-coordinate and the B–N bond distances are approximately equal (*ca.* 1.43 Å) in the solvent-separated ion pairs **18** and **19** [41].

As indicated in Scheme 15, the mono-*bam* complexes Ph(μ-N^{t}Bu)$_2$AlCl(OEt$_2$) (**10**) and [Ph(μ-N^{t}Bu)$_2$MCl]$_2$, M = Ga (**11**), M = In (**12**) are intermediates in the formation of **13**–**15**. Indeed, in the case of aluminum, it is preferable to isolate **10** prior to reaction with the second equivalent of Li$_2$[Ph(μ-N^{t}Bu)$_2$], in order to optimize the yield of **13** [24]. The M–Cl functionality in these group 13 complexes provides an opportunity to install an alkyl group on the metal center. By analogy with related aluminum *am* complexes [16–22], the alkene polymerization activity of the resulting aluminum *bam* complexes is of potential interest.

Only one study to date has been carried out to produce boraamidinate complexes of the heaviest member of group 13. The dithallium(I) complexes Tl$_2$[PhB(μ$_3$-NR′)$_2$] (**17**) (R′ = ^{t}Bu, ^{i}Pr) were synthesized by the reaction of the corresponding dilithium boraamidinate complex with thallium(I) chloride (Scheme 16) [42]. X-ray characterization of these complexes has shown that the ligand adopts the bridging bonding mode **E**. This is the same bonding mode observed in the analogous dilithium complexes (Chart 6) and the metrical parameters of the ligand remain unchanged on coordination to thallium. However, instead of forming dimeric or trimeric aggregates in the solid state through metal–nitrogen contacts, the thallium complexes assume extended structures through weak intermolecular thallium–thallium contacts (R = ^{t}Bu, 3.228(3)–3.772(2) Å; R = ^{i}Pr, 2.950(2)–3.553(2) Å). In the case of the *iso*-propyl derivative, there are an increased number of intermolecular metal–metal contacts, which are shorter when compared to those in the *tert*-butyl derivative. This is presumably a result of the reduced steric interactions that allow the molecules to pack closer together.

The one-electron oxidation of the monoanions **13**–**15** with iodine produces the neutral radicals {M[PhB(μ-N^{t}Bu)$_2$]$_2$}$^\bullet$ [M = Al (**71**), Ga (**72**), In (**73**)] (Scheme 17). The Al and Ga complexes, **71** and **72**, can be isolated as dark red or dark green crystals, respectively, that are stable under an inert atmosphere for months [24]. In contrast, the dark green complex **73** has only been characterized in solution [46].

Theoretical calculations on the D_{2d} symmetric diamagnetic model systems {M[PhB(NMe)$_2$]$_2$}$^-$ (M = B [46], Al [24], Ga [24], In [46]) showed that the HOMOs transform as the a$_2$ irreducible representation in the D_{2d} point group (Fig. 2). Thus, a one-electron oxidation yields the corresponding neutral radicals {[PhB(NMe)$_2$]$_2$M}$^\bullet$ with ^{2}A$_2$ ground state and D_{2d} symmetry (Fig. 2).

The model systems predict that the spirocyclic radicals **71**–**73** would retain the D_{2d} symmetry of their parent diamagnetic anions {M[PhB(μ-N^{t}Bu)$_2$]$_2$}$^-$. This was confirmed by X-ray structural analyses of **71** and **72** that reveal only slight deviations from the idealized structures. In the solid state, **71** and **72** lie on a crystallographic two-fold axis that imposes crystallographic equivalence on the two *bam* ligands. The four-membered BN$_2$M rings are essentially planar and are orthogonal to each other. The metrical parameters of the *bam* ligands in these two radicals are identical within experimental error (Table 1). The

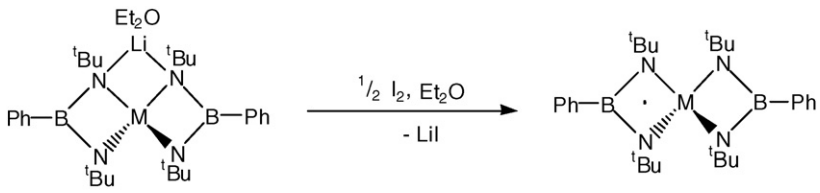

13 M = Al
14 M = Ga
15 M = In

71 M = Al
72 M = Ga
73 M = In

Scheme 17.

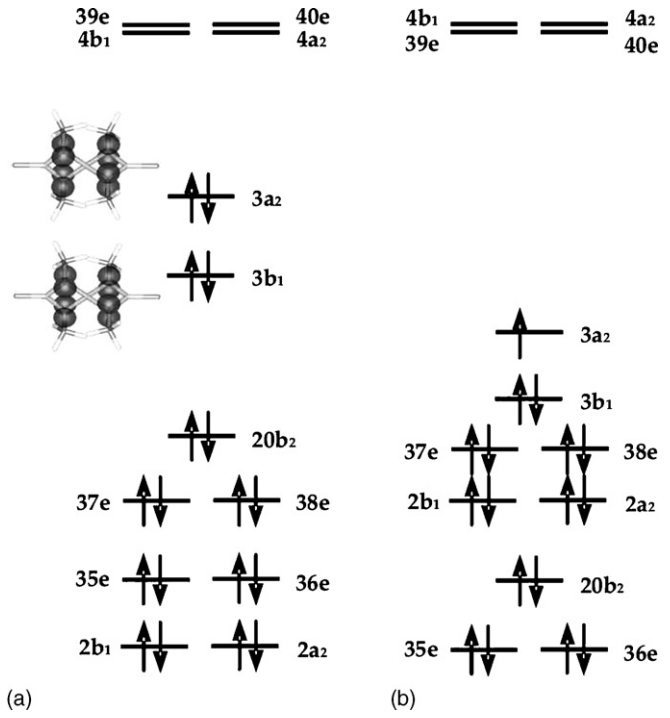

Fig. 2. Schematic frontier orbital diagrams of (a) $\{[PhB(NMe)_2]_2Al\}^-$ and (b) $\{[PhB(NMe)_2]_2Al\}^\bullet$ [24]. Reproduced by permission of The Royal Society of Chemistry.

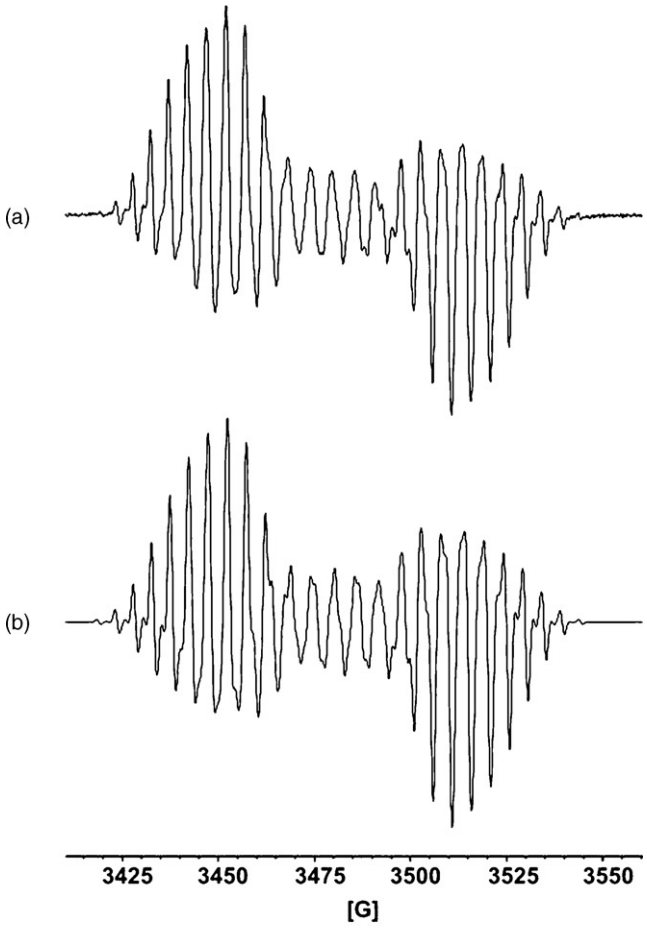

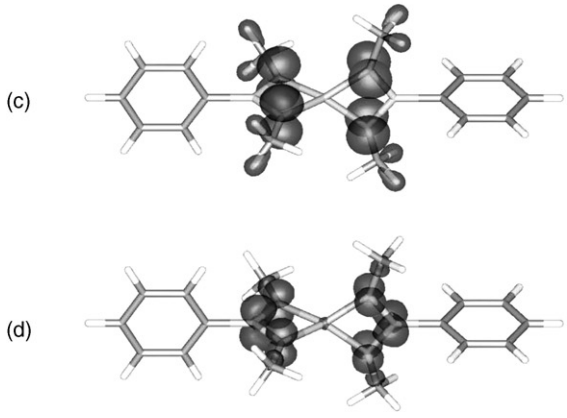

Fig. 3. Experimental (a) and simulated (b) X-band EPR spectra of a diethyl ether solution of $\{Al[PhB(\mu\text{-}N^tBu)_2]_2\}^\bullet$ (**71**) at 298 K. (c) The SOMO of $\{Al[PhB(\mu\text{-}NMe)_2]_2\}^\bullet$ drawn at isosurface level ±0.05. (d) Spin density map of $\{Al[PhB(\mu\text{-}NMe)_2]_2\}^\bullet$ drawn at isosurface levels 0.02 (α-spin density) and −0.002 (β-spin density) [24]. Reproduced by permission of The Royal Society of Chemistry.

geometry about the central metal atom is distorted tetrahedral, 76.37(9)–128.5(1)° in **71**, 72.81(9)–130.9(1)° in **72**, as a result of geometric constraints imposed by the *bam* ligands. The NBN angles of the *bam* ligands (104.2(2)° in **71**, 104.7(2)° in **72**) are the smallest observed of all the bis-*bam* spirocycles adopting bonding mode **C**, most likely due to the relatively small size of the metal centers.

Single point calculations for the model radicals $\{M[PhB(NMe)_2]_2\}^\bullet$ (M = B, Al, Ga, In) in their optimized geometries have shown their SOMOs consist solely of nitrogen p-orbitals and are equally delocalized over all four nitrogen atoms (Fig. 3(c)). Furthermore, Mulliken population analysis revealed the spin density to be equally distributed among all nitrogen centers (Fig. 3(d)). Although the SOMOs do not include contributions from boron or from the central metal, these atoms also have non-zero spin density values arising from spin polarization effects as revealed in their EPR spectra (Figs. 3 and 4). The experimental EPR spectra of the spirocyclic radicals **71**–**73** can be simulated by assuming hyperfine interaction of the unpaired electron with the central metal (^{27}Al, I = 5/2, 100%; ^{69}Ga, I = 3/2, 60.1%; ^{71}Ga, I = 3/2, 39.9%; ^{113}In, I = 9/2, 4.3%; ^{115}In, I = 9/2, 95.7%), two equivalent boron atoms, and four equivalent nitrogen centers [23,43]. Hence, the spectral simulations and DFT calculations indicate uniform spin delocalization throughout both *bam* ligands in these radicals, and confirm the retention of spirocyclic structures in solution.

In an attempt to synthesize the boron analogue of **13**–**15**, the reaction of $Li_2[PhB(\mu\text{-}N^tBu)_2]$ with $BF_3{\cdot}OEt_2$ in a 2:1 molar ratio was investigated [46]. This synthetic approach is not as straightforward as observed for complexes **13**–**15**. NMR spectroscopic analysis of the reaction mixture revealed the existence of more than one reaction pathway. The borazine $[PhF_2B_3N_3{}^tBu_3]$ (**74**) has been isolated from this reaction and characterized by X-ray crystallography and multinuclear NMR spectroscopy [46,70]; *cf.* formation of the borazine $[Ph_3B_3N_3Me_3]$ (**53**) (Scheme 10) [33]. Formation of the monolithiated spirocyclic *bam* complex $Li(Et_2O)B[PhB(N^tBu)_2]_2$

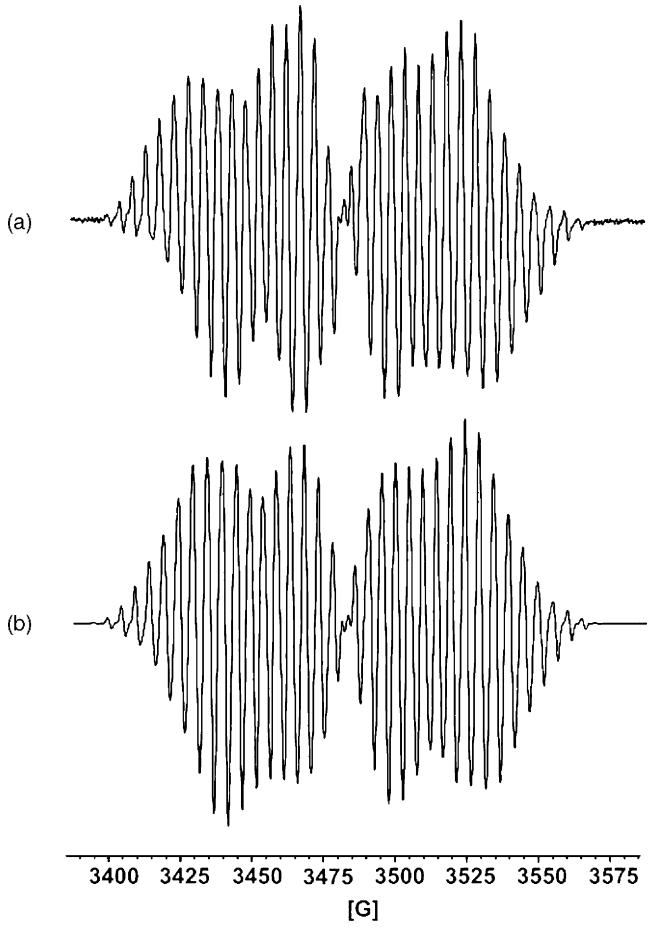

Fig. 4. Experimental (a) and simulated (b) X-band EPR spectra of a diethyl ether solution of $\{Ga[PhB(\mu\text{-}N^tBu)_2]_2\}^\bullet$ (**72**) at 298 K [24]. Reproduced by permission of The Royal Society of Chemistry.

(**75**) is indicated on the basis of multinuclear NMR spectra. Further evidence is provided by the EPR spectroscopic investigations of the bright purple diethyl ether solution formed upon oxidation (Scheme 18). This confirmed the presence of the persistent spirocyclic radical $\{B[PhB(\mu\text{-}N^tBu)_2]_2\}^\bullet$ (**76**) [46].

4.2.2. Silicon, germanium, tin, and lead

Bam complexes of all four group 14 elements have been reported. They adopt a variety of bonding modes, **A**, **B**, **C**, **E** or **F** in the solid state (Chart 5). A mixed lithium and lead complex displays a unique trimetallic bridging mode. The two structurally characterized examples of *bam* derivatives of silicon take the same form, with the ligand adopting bonding mode **A** (Chart 8) [31,37]. The syntheses of complexes **46** and **57** are outlined in Sections 2.4 and 2.6, respectively. As indicated in Table 1, the parameters of the boraamidinate ligand show delocalised B–N bonding with B–N bond lengths in the narrow range 1.436(6)–1.450(5) Å. The N–B–N angles in **46**, 101.6(4)°, and **57**, 102.5(2)°, are considerably compressed from the ideal trigonal planar geometry due to coordination to the small silicon center.

Metathesis reactions of dilithio *bams* with group 14 halides have led to the characterization of bis-*bam* complexes of germanium (**20**) and tin (**21**), in which the ligand would be expected to exhibit bonding mode **C** [27,38]. However, these complexes have yet to be characterized in the solid state.

The reaction of dilithio *bams* with one equivalent of a dimethyltin dihalide affords complexes **31** and **32**. It has been shown, in the case of this reaction, that the bonding mode adopted by the *bam* ligand is dependent on the steric bulk of the substituents on nitrogen. A dimeric complex **31** with bridging *bam* ligands, bonding mode **F**, is preferred for R = Me and Et. However, with bulkier groups on the *bam* ligand, a monomeric complex, **32**, is observed [27,32,38].

A more unusual synthesis of a tin *bam* complex, **59**, involving metathesis followed by the elimination of BMe_3 [25], is depicted in Scheme 12. The dimeric product observed adopts bonding mode **B** and is isostructural with the lead complex $\{Pb[PhB(\mu_3\text{-}N^tBu)(\mu\text{-}N^tBu)]\}_2$ (**24**). Interestingly, the synthesis of **24** initially involved the reaction of two equivalents of $Li_2[PhB(N^tBu)_2]$ with $PbCl_4$. However, reduction of the metal center occurs to give the dimeric lead(II) complex, which may also be obtained by using $PbCl_2$ [28]. Solution NMR data of **24**, which adopts a dimeric structure in the solid state, are consistent with dissociation into two monomers [28]. Mass spectrometry

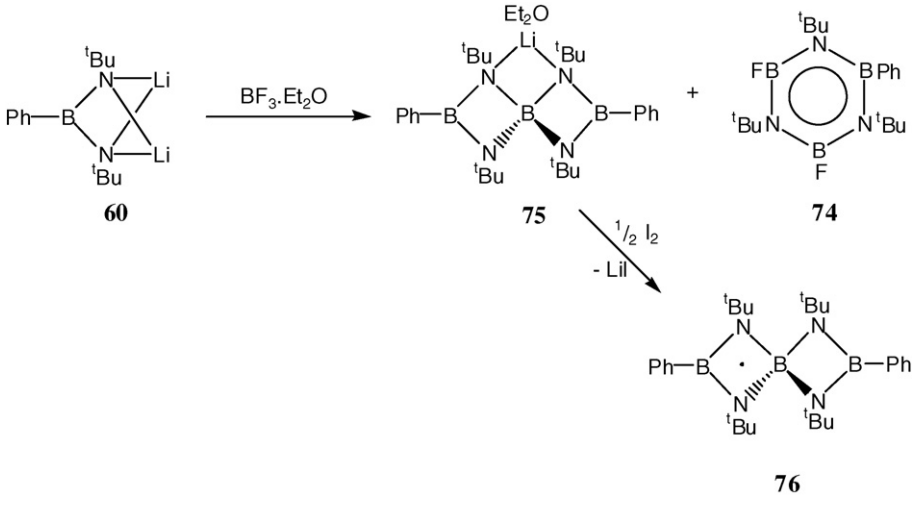

Scheme 18.

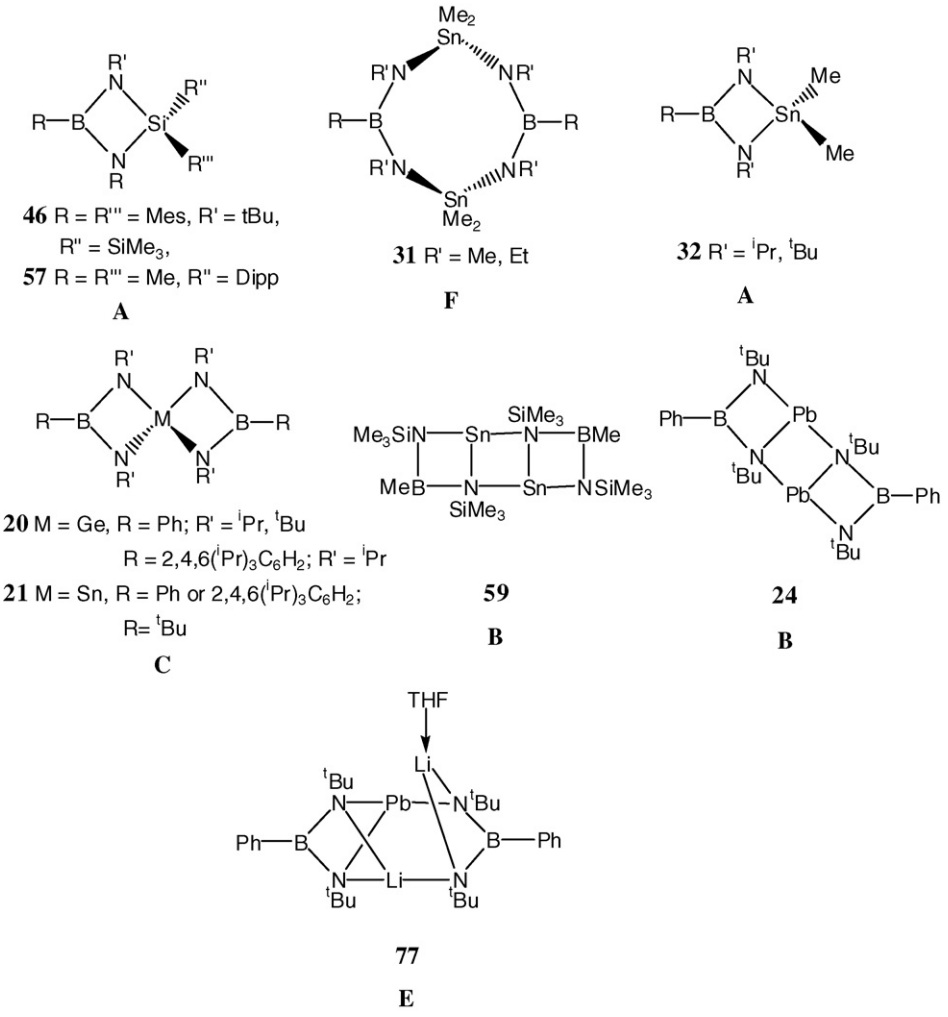

Chart 8.

also indicates that this lead(II) complex breaks up in the gas phase. The related tin(II) complex **59** exhibits fluxional behavior above 333 K in solution [25].

The bis-*bam* lead(II) complex Li(THF)LiPb[PhB(μ_3-N^{t}Bu)$_2$]$_2$ (**77**) has recently been prepared by the reaction of PbI_2 with two equivalents of Li_2[PhB(N^{t}Bu)$_2$] [46b]. Interestingly, one of the *bam* ligands bridges the Pb atom and the unsolvated Li ion (bonding mode **E**) while the second *bam* ligand exhibits a unique motif, bridging all three metal centres.

4.2.3. Phosphorus, arsenic, antimony and bismuth

Several phosphorus *bam* derivatives have been characterized in the solid state. All of these are mono-*bam* systems that adopt bonding mode **A** (Table 1). Recently, a series of *bam* complexes has been prepared and structurally characterized for the heavier group 15 elements (As, Sb and Bi), in which the ligand displays a variety of coordination modes [40b].

The complexes [PhB(μ-N^{t}Bu)$_2$]PX (**25**) (X = Br, Cl) [40a] were synthesized by metathesis of Li_2[PhB(N^{t}Bu)$_2$] with one equivalent of the corresponding phosphorus trihalide. The isolation of these mono-substituted complexes provides an opportunity to further functionalize the main-group element center. For example, reaction of **25** (X = Cl) with lithium *tert*-butylamide affords the mono-*bam* [PhB(μ-N^{t}Bu)$_2$]PN(H)^{t}Bu (**78**). Deprotonation with *n*-butyl lithium, generates the corresponding monolithiated derivative {[PhB(μ_3-N^{t}Bu)(μ-N^{t}Bu)]P(μ_3-N^{t}Bu)Li}$_2$ (**79**), that forms a dimer in the solid state via Li–N interactions (Scheme 19) [40]. The PNBN ring contains one three-coordinate nitrogen and one four-coordinate nitrogen atom resulting in a disparity between B–N bond lengths, 1.418(2) and 1.476(2) Å, within the *bam* ligand.

The reactions of Li_2[PhB(N^{t}Bu)$_2$] with ECl_3 (E = As, Sb and Bi) in a 1:1 molar ratio in diethyl ether produce the mono-*bam* derivatives PhB(μ-N^{t}Bu)$_2$ECl, **26**–**28** in 55–75% yields [40b]. When the same reaction is carried out in a 2:1 molar ratio in boiling diethyl ether, the complexes LiE[PhB(μ-N^{t}Bu)(μ_3-N^{t}Bu)]$_2$ **80** (E = As) and **81** (E = Sb) are obtained in 55–85% yields. The unsolvated compounds have a ladder structure, a similar structural motif to that of the dimeric Pb(II) complex **24**. Solvation of the Li ion by a diethyl ether molecule in the arsenic derivative Li(OEt_2)As[PhB(μ-N^{t}Bu)$_2$][PhB(μ_3-N^{t}Bu)(μ_3-N^{t}Bu)] (**82**) results in the loss of the transannular Li–N bond to give a bicyclic structure comprised of a four-membered BN_2As and a six-membered BN_3AsLi ring

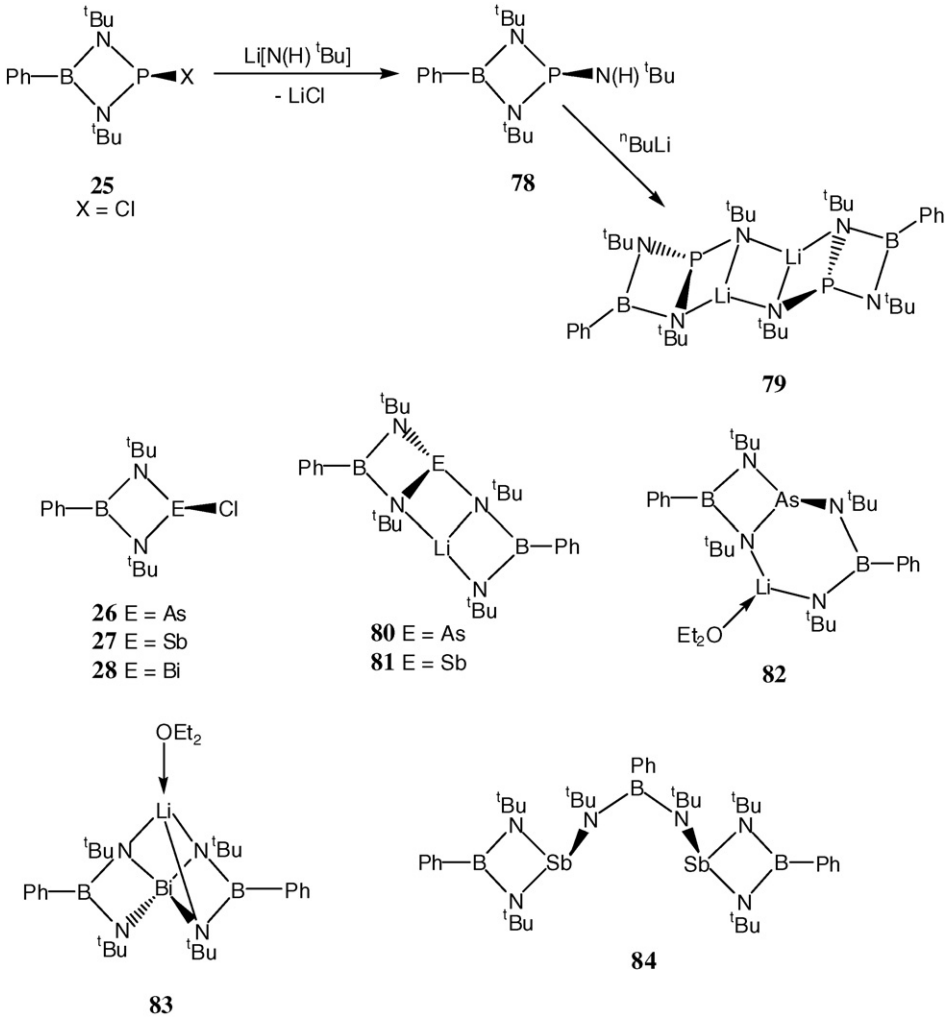

Scheme 19.

[40b]. By contrast, in the corresponding mono-solvated bismuth complex **83**, both the solvated Li ion and the bismuth center become four-coordinate resulting in a tetracyclic structure [40b].

The derivative $\{Sb[PhB(\mu\text{-}N^tBu)_2]_2\}[\mu\text{-}PhB(N^tBu)_2]$ (**84**) is isolated in 58% yield from the reaction of $Li_2[PhB(N^tBu)_2]$ with $SbCl_3$ in a 2:1 molar ratio in diethyl ether after a short reaction time at room temperature [40b]. In this unique complex each antimony center is *N*,*N*′-chelated by a *bam* ligand and the two $[Sb(bam)]^+$ units are bridged by a third $[bam]^{2-}$ ligand. Thus, this dinuclear complex combines bonding modes **A** and **F**.

4.2.4. Sulfur and tellurium

Bam complexes of group 16 elements, especially sulfur, have been extensively characterized in solution. The calculated ^{11}B NMR chemical shifts for $S[PhB(\mu\text{-}NH)_2]$ and related model systems by the IGLO method gave acceptable correlations with experimental values [30]. Examination of Table 1 shows that five *bam* complexes have been characterized by X-ray crystallography, four of which adopt bonding mode **A** (Chart 9 and Scheme 20). The mononuclear group 16 complexes **45** and **51** both contain almost planar ENBN (E = S, Te) rings [30,36]. Only one bis-*bam* complex $Te[PhB(\mu\text{-}N^tBu)_2]_2$ (**85**), which adopts

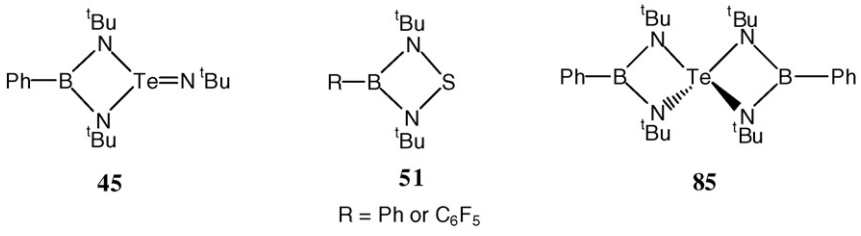

Chart 9.

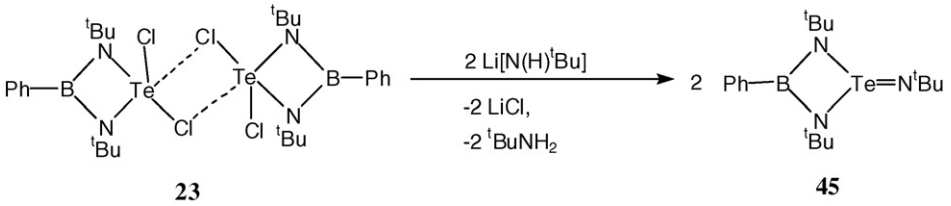

Scheme 20.

bonding mode **C**, has been characterized in the solid state [34]. The B–N bond distances in the ligands of these group 16 complexes are very similar and fall in the range 1.417(4)–1.46(1) Å. The NBN and NMN angles are larger for the tellurium complexes reflecting the increased size of the bite angle required for coordination.

The tellurium complex $\{[PhB(\mu\text{-}N^tBu)_2]TeCl_2\}_2$ (**23**) forms a centrosymmetric dimer linked by weak Te···Cl interactions [3.2411(6) Å] in the solid state (Scheme 20) [40]. The Te atom is in a distorted pseudo-octahedral environment, with the lone pair occupying one of the octahedral sites. Treatment of **23** with two equivalents of lithium *tert*-butylamide produces the mono-*bam* complex $[PhB(\mu\text{-}N^tBu)_2]Te{=}N^tBu$ (**45**), a rare example of a monomeric tellurium imide, in 40% yield. The initial step of this transformation presumably involves nucleophilic substitution of the two chloride substituents by ^{t}BuNH groups, which is then followed by elimination of ^{t}BuNH$_2$ (Scheme 20) [40].

4.3. d-Block metal complexes

Early investigations of the coordination chemistry of *bam* ligands to transition metals were limited to group 4 with only mono- and bis-*bam* complexes characterized. A more recent examination of early transition-metal complexes has revealed tris-*bam* complexes (group 4) or examples where three *bam* ligands bridge a M≡M unit (group 6) (Chart 4).

4.3.1. Titanium, zirconium and hafnium

There are several structurally characterized examples of group 4 metal complexes of the boraamidinate ligand. This has mostly been driven by the interest in these metals for their catalytic activity and the search for novel ligand systems to enhance this property.

Monoboraamidinate complexes of the form $R_2M[PhB(\mu\text{-}N^tBu)_2]$ are known for titanium (**33**) and zirconium (**34**), with the ligand adopting bonding mode **A** (Chart 10). These complexes are synthesized by metathesis of the parent lithium complex **2**, with the appropriate organometallic group 4 halide. Reaction of two equivalents of the dilithio derivative **2** with the appropriate metal tetrachloride affords the neutral spirocyclic complexes $M[PhB(\mu\text{-}N^tBu)_2]_2$, M = Ti (**35**) [27] and $M[PhB(\mu\text{-}N^tBu)_2]_2(THF)$, M = Zr (**36**), Hf (**37**) [43]. Complexes **36** and **37** contain square-pyramidal metal centers with a molecule of THF occupying the fifth coordination site. This is in contrast to the titanium complex, **35**, which has an unsolvated four-coordinate metal center. This could be due to the smaller titanium center preferring a four-coordinate geometry, however it cannot be overlooked that **36** and **37** were both synthesized using the solvated $MCl_4(THF)_2$ complexes, whereas **36** was prepared from unsolvated $TiCl_4$. The metrical parameters of the *bam* ligand in complexes **35**–**37** do not change significantly with the increasing size of the metal center. For example, the NMN angles are 70.5(2)° in **36** and 71.0(2)° in **37**, and the NBN angle of 111.2(4)° exhibited by both complexes is similar to that observed for the unsolvated titanium derivative **35** [110.5(6)°] [27].

Trisboraamidinate complexes, $Li_2[M\{PhB(\mu\text{-}N^tBu)_2\}_3]$, M = Zr (**38**), M = Hf (**39**), can also be synthesized by metathesis for the larger group 4 metals. In these cases, the metal(IV) center is octahedral, surrounded by three *bam* ligands, producing dianions which possess pseudo-D_3 symmetry. The inclusion of the two Li^+ counterions, however, lowers the symmetry of the molecules to pseudo-C_2. In two of the *bam* ligands, one N atom is in close contact with a single lithium cation, while the other connects with both lithium cations leading to longer B–N bond lengths compared to those in the third ligand or in the spirocyclic bis-*bam* complexes **36** and **37** [43].

Associated structures involving halide bridges are observed for some mono-*bam* complexes containing metal-halogen functionalities. An interesting example is the titanium complex $\{Ti(\mu\text{-}Cl)_2[PhB(\mu\text{-}N^tBu)_2]\}_n$ (**86**), obtained by treatment of $Ti(NMe_2)_2[PhB(\mu\text{-}N^tBu)_2]$, **33**, with two equivalents of Me_3SiCl (Scheme 21). This complex forms polymeric chains propagated by bridging chlorides to give pseudo-octahedral geometry around the titanium centers [44]. Complex **86** can then be converted to the corresponding dibenzyl

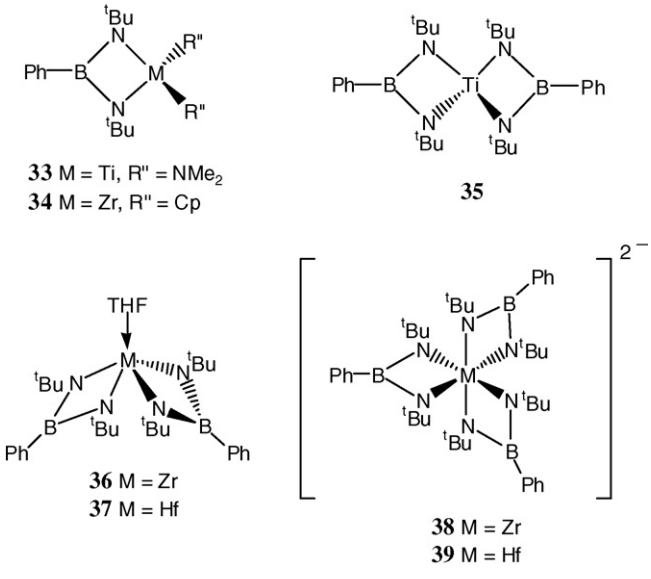

Chart 10.

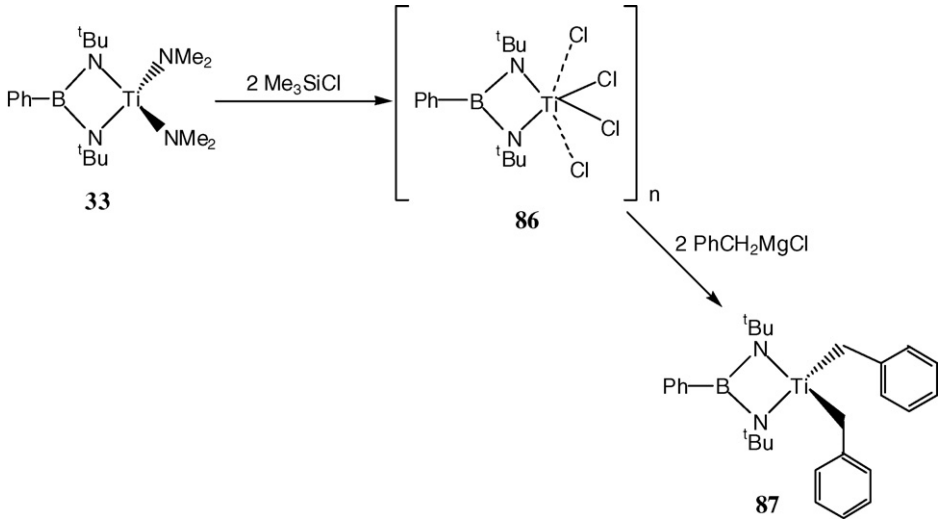

Scheme 21.

derivative Ti[$(CH_2Ph)_2$[$(PhB(\mu\text{-}N^tBu)_2$] (**87**), by reaction with $PhCH_2MgCl$ (Scheme 21) [44].

The replacement of cyclopentadienyl ligands on titanium or zirconium dialkyls with chelating dianionic ligands is an area of current interest in the design of olefin polymerization catalysts. To date, there has been only one preliminary investigation of the effect of the electrophilic boron center in a *bam* ligand on the catalytic behavior of metal complexes. The activation of **87** with $[Ph_3C][B(C_6F_5)_4]$ followed by addition of 200 equiv. of 1-hexene at room temperature showed no formation of poly(1-hexene) [44]. The observed lack of polymerization activity was attributed to insertion of a single olefin into the titanium–benzyl bond, or the extreme electrophilicity of the titanium center engendered by the presence of boron at the bridgehead of the *bam* ligand. By contrast, the complexes $DippNB(NMe_2)B(NMe_2)NDippTiR_2$ (R = Me, CH_2Ph) **88** (Chart 11), which incorporate a B–B linkage into a diamide backbone, behave as polymerization catalysts upon activation [71].

Several complexes in which the *bam* anion radical $[PhB(N^tBu)_2]^{-\bullet}$ is stabilized by complexation to an early main-group metal center have been reported, as discussed in Section 4.2. These findings suggest that redox behavior is an important feature of these boron-containing systems. In this context, the unsuccessful attempts to prepare titanium(IV) complexes by transamination of $Ti(NMe_2)_4$ with $PhB[N(H)^tBu]_2$ or the reaction of $Li_2[PhB(N^tBu)_2]$ with $TiCl_4$ are noteworthy [44]. The former reaction produces "significant amounts of reduced titanium product and only small amounts" of $Ti(NMe_2)_2[PhB(\mu\text{-}N^tBu)_2]$, **33**. However, the orange complex **33** is obtained in 45% yield by treatment of $Ti(NMe_2)_2Cl_2$ with $Li_2[PhB(N^tBu)_2]$. The reduction of Ti(IV) to Ti(III) is again indicated by the formation of a green by-product, presumably accompanied by the oxidation of the *bam* dianion $[PhB(N^tBu)_2]^{2-}$ to the radical anion $[PhB(N^tBu)_2]^{-\bullet}$. In general, redox behavior must be considered as a possible outcome in metathetical reactions between *bam* dianions $[RB(NR')_2]^{2-}$ and metal halides that are in higher oxidation states.

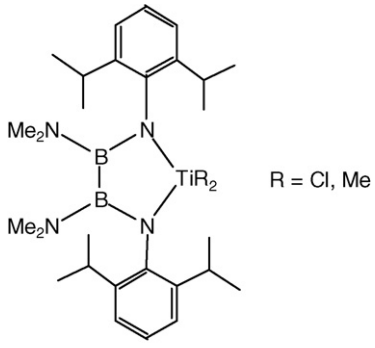

Chart 11.

4.3.2. Vanadium

The coordination chemistry of group 5 metals with the *bam* ligand is limited to a single example. The paramagnetic blood-red complex $V[PhB(\mu\text{-}N^tBu)_2]_2$ (**42**) [43] exhibits a strong EPR signal at room temperature with no hyperfine coupling. However, a frozen pentane solution (77 K) gives a resolved octet in the EPR spectrum arising from the interaction of the unpaired electron with one vanadium nucleus (^{51}V, $I = 7/2$, 99.8%, $g = 1.979$, $A(^{51}V) = 49.0$ G). The significant line broadening and increased amplitude in the first and final peaks were attributed to hyperfine coupling to the quadrupolar nitrogens. A simulated spectrum (Fig. 5) was found to be in accordance with the experimental spectrum yielding $A(^{14}N) = 4.7$ G. In contrast to the paramagnetic early main-group metal *bam* complexes in which the spin density was found to be mainly ligand-based, the paramagnetic species **42** is a V(IV) complex of two diamagnetic *bam* dianions $[PhB(N^tBu)_2]^{2-}$.

The absorption spectrum of **42** was found to be consistent with a d^1 metal center in a tetrahedrally distorted crystal field. The ^2E and $^2T_2$ terms of T_d symmetry are split in D_{2d} symmetry to a $^2B_1$ ground state and $^1A_1$, $^2B_2$, and ^2E excited states. For these three excited states, the $^2E \leftarrow {}^2B_1$ transition is Laporte-

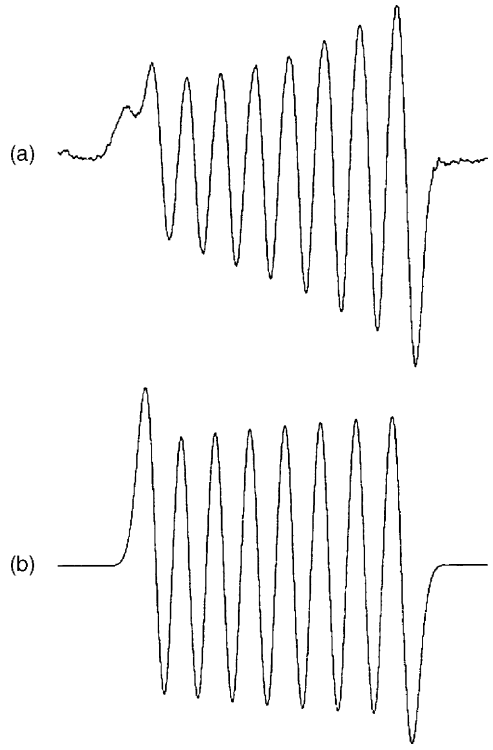

Fig. 5. EPR spectrum of V[PhB(μ-N^{t}Bu)$_2$]$_2$ (**42**) at 77 K in frozen pentane: experimental (a); simulated (b) [43]. Reproduced with permission from [43]. Copyright 2003 American Chemical Society.

allowed. A ligand to metal charge-transfer (LMCT) transition at 260 nm was reported to dominate the UV absorption region.

4.3.3. Molybdenum and tungsten

Four group 6 *bam* complexes, M≡M[PhB(NR′)$_2$κ^2*N*,*N*′]$_3$ (M = Mo, W, R′ = Et, ^{i}Pr), have been reported, two of which have been structurally characterized in the solid state (M = Mo, R′ = Et, **40**; M = W, R′ = ^{i}Pr, **41**) (see Chart 4 and Table 1) [45].

The NMMN torsion angles (*ca.* 0.2–1.6°) indicate nearly eclipsed ligand geometry, while the coordination environment of each metal center is nearly trigonal pyramidal [∠NMN 93.1(2)–94.6(1)°]. Although the bond lengths of the *bam* ligands in this bonding mode are similar to those observed when the *bam* ligands chelate a single metal center, the NBN bond angles are larger, 117.0(3)–l 18.0(8)°, since the ligand is spanning a dinuclear M=M unit. The group 6 complexes are further distinguished by the shortest metal-metal distances, 2.1612(6) Å (**40**), 2.2351(7) Å (**41**), observed for neutral M_2X_6 species to date. The determining factor contributing to the short metal–metal bond lengths and small torsional distortion is the steric constraint imposed by the three-atom NBN backbone of the *bam* ligand.

DFT calculations were performed on model Mo and W complexes in which methyl groups were used as alkyl substituents and the geometry was constrained to D_{3h} symmetry [45]. Good agreement between the calculated and observed structures was obtained. The energy levels and frontier orbitals revealed (a) the HOMO is a N p-based orbital, (b) strong metal–metal character in HOMO-1 for Mo and HOMO-2 for W, and (c) a large HOMO-LUMO gap for both model complexes. The latter feature is manifested in the absorption spectra of these tan complexes, which are dominated by a single, intense band at 310 nm. The chemical properties of **40** and **41** were also found to be consistent with the calculated electronic structure. These complexes do not react with σ-donor ligands or with chalcogen-transfer reagents, in accordance with the ligand-based HOMO and the high energy of the LUMO. However, they are susceptible to oxidation, as indicated by their pyrophoric nature when exposed to air.

4.3.4. Zinc and cadmium

The dilithiated spirocyclic group 12 complexes [Li(Et$_2$O)]$_2$-[M{PhB(μ$_3$-N^{t}Bu)$_2$}$_2$] (**43**, M = Zn [46a]; **44**, M = Cd [46b]) are isostructural with the magnesium analogue **9**. The zinc derivative **43** exhibits similar redox behavior upon oxidation with iodine (Scheme 22), resulting in the formation of the bright purple radical {Li(Et$_2$O)Zn[PhB(μ-N^{t}Bu)$_2$][PhB(μ$_3$-N^{t}Bu)$_2$]}$^\bullet$ (**89**) [46a].

The EPR spectrum of this radical exhibits a similar hyperfine pattern to that of the magnesium analogue owing to the low natural abundances of the spin-active isotopes for magnesium and zinc [46]. The experimental spectrum may be simulated by invoking hyperfine structure resulting from interaction of the unpaired electron with two inequivalent nitrogen atoms, the central metal (^{67}Zn, I = 5/2, 4.1%), and one boron atom (Fig. 6). DFT calculations confirm that **89** adopts a C_s-symmetric structure in solution with localized spin density on the *bam* ligand that is not coordinated to lithium (Fig. 6).

5. NMR solution spectra

The vast majority of *bam* complexes exhibit a broad resonance in the ^{11}B NMR spectrum in the range 28–40 ppm characteristic of a three-coordinate boron center [72]. Notable exceptions include (a) tris-*bam* complexes **40** and **41** (Chart 3) in which the *bam* ligand bridges a dinuclear M=M unit (M = Mo, W) giving rise to ^{11}B chemical shifts of 50–52 ppm [45] and (b) the mono-*bam* complexes Cp$_2$Zr[PhB(μ-N^{t}Bu)$_2$], **34** [27] and

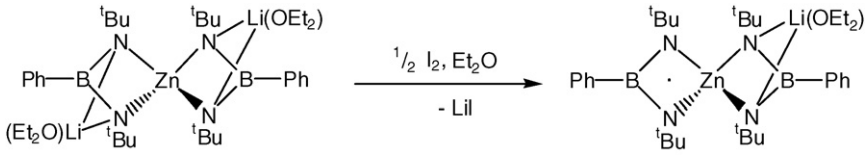

43 **89**

Scheme 22.

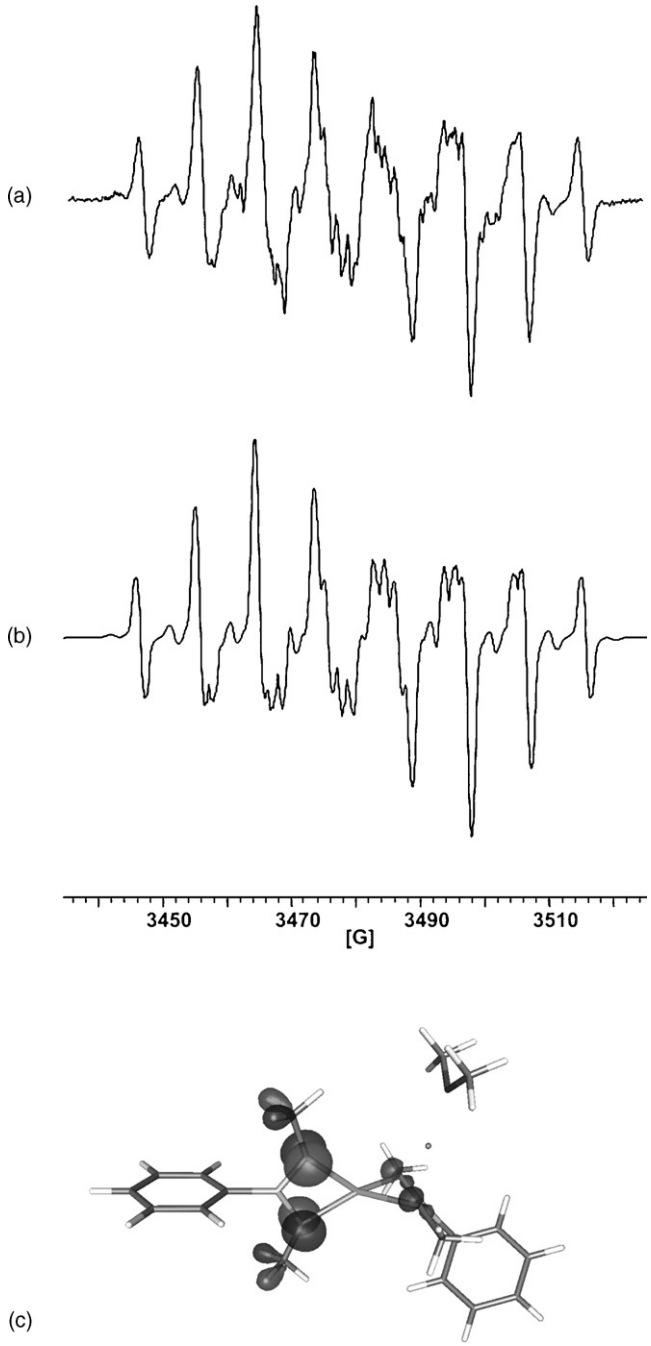

Fig. 6. Experimental (a) and simulated (b) X-band EPR spectra of a diethyl ether solution of $\{Li(Et_2O)Zn[PhB(\mu\text{-}N^tBu)_2]_2\}^\bullet$ (**89**) at 25 °C; (c) SOMO (isosurface values ±0.06) of $\{Li(Me_2O)Zn[PhB(\mu\text{-}NMe)_2]_2\}^\bullet$. Reproduced with permission from [46a]. Copyright 2006 American Chemical Society.

$S[C_6F_5B(\mu\text{-}N^tBu)_2]$, **51** [29], for which values of 20 ppm are reported.

For most *bam* metal complexes, solution NMR data are in accordance with the structures observed in the solid state. For example, the ^1H NMR spectra of the dinuclear complexes **40** and **41** (Chart 4) in C_6D_6 reveal only one environment for the alkyl (ethyl or *iso*-propyl) and phenyl groups consistent with the preservation of D_{3h} symmetry observed in the solid state [45].

In a few cases, NMR spectroscopic studies have indicated that the associated structures observed in the solid state are disrupted in solution. For example, multinuclear NMR spectroscopic data at ambient temperature in d_8-THF for $\{Li[PhB(\mu_3\text{-}N^tBu)(\mu\text{-}N^tBu)]P(\mu_3\text{-}N^tBu)\}_2$ (**79**), which adopts a dimeric structure in the solid state, indicates disruption of the dimeric structure that is most likely caused by solvation of the Li^+ centers by THF [40]. Similarly, the dimeric lead(II) complex **24** is thought to dissociate in solution on the basis of NMR data (Section 4.2.2).

6. Hybrid boraamidinate-amidinate (*bamam*) ligands

Finally, a related class of ligand will be discussed, which is a hybrid of the boraamidinate (*bam*) and amidinate (*am*) ligands, designated as the *bamam* ligand [41]. The discovery of a direct synthesis to mono-amino reagents of the type **3** [41] stimulated attempts to generate *bamam* ligands that are formally isoelectronic with the extensively studied *nacnac* (β-diketiminate) ligands. These investigations are of fundamental significance since, although the coordination chemistry of the *nacnac* ligand has been widely studied [49], less emphasis has been placed on examining the effect of altering the backbone of this ligand [41,48].

The preparation of protio *bamam* derivatives **90** and **92**, in good yields, has been attained by two different routes (Scheme 23) [41]. The first makes use of the reaction of lithium *ams* with the mono-aminochloroborane **3**. The second synthetic approach involves nucleophilic replacement of the exocyclic chloro substituent in $PhB(Cl)[RC(\mu\text{-}NR')_2]$ (**91**) [73] by an amino group. The protonated *bamam* derivatives may form either four-membered BNCN rings with an exocyclic amido substituent (**92**) or acyclic NBNCN structures (**90**), depending on the substituents on the backbone of the ligand. Protio *nacnac* ligands adopt acyclic structures exclusively [49]. In contrast, the presence of the electron-accepting boron atom in the *bamam* backbone can promote the formation of cyclic BNCN systems. Monolithiation of the exocyclic amido substituent on the ring system in **92** generates the alkali derivative $Li[DippN(Ph)B(N^tBu)C^nBu(N^tBu)\text{-}N,N']$ (**93**, $R' = {}^t$Bu, $R'' = {}^t$Bu, $R'' =$ Dipp) (Scheme 23) [41]. Compounds of the type **91** are prepared by the metathesis reactions of $PhBCl_2$ with the appropriate lithium amidinate [73–76]. An alternative route involves the insertion reaction of a carbodiimide, e.g. CyN=C=NCy, with $RBC1_2$ (R = Ph, $N(SiMe_3)_2$) [74,75] or $FcBr_2$ (Fc = ferrocenyl) [76].

Both **92** and **93** can serve as effective reagents for the installation of the *bamam* ligand on a metal site [48]. Organomagnesium complexes of the type **94** have been obtained in 58–79% yields by treatment of **93** with Grignard reagents, or by the reaction of **92** with dibutylmagnesium (Scheme 24). Six examples of the organomagnesium complexes **94** have been characterized in the solid state.

In *N*,*N*′-chelated metal *nacnac* complexes, the six-membered metallacycle is usually planar, although distortions toward a boat structure are sometimes observed as a result of steric crowding around the metal center [49]. X-ray structural analyses of **94** have revealed that there is a substantial interaction between the central

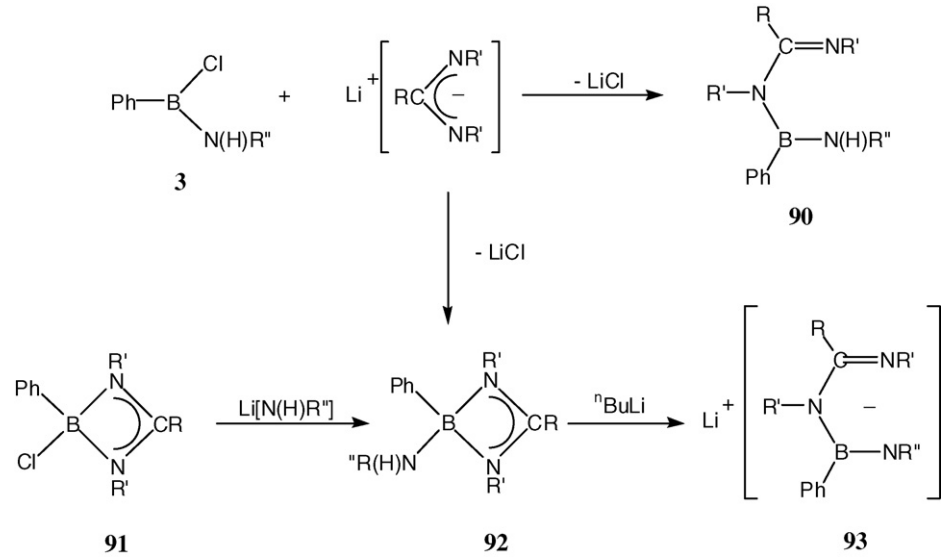

Scheme 23.

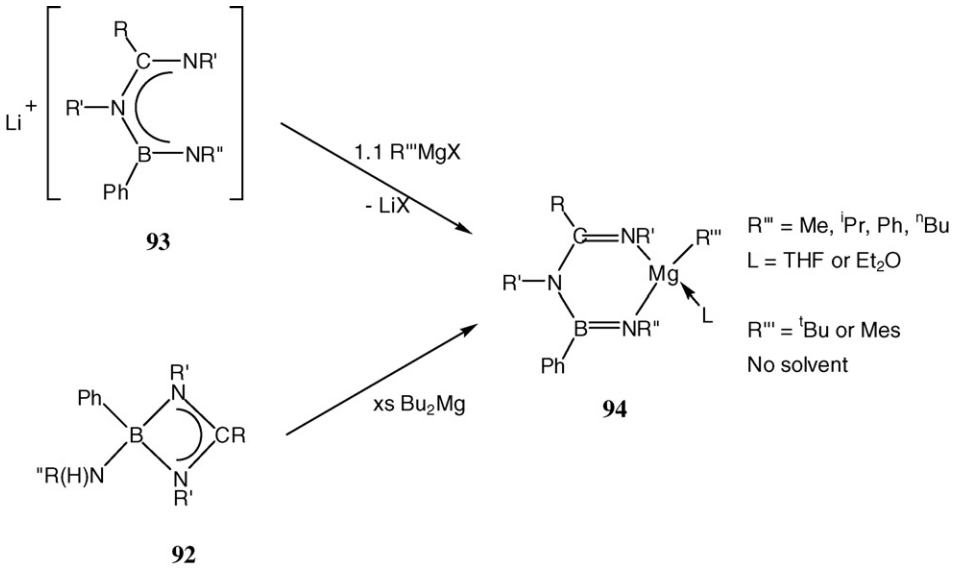

Scheme 24.

nitrogen atom of the *bamam* ligand and the unsolvated magnesium centers [48]. The magnitude of the transannular Mg–N interaction in these complexes is similar to the value of a typical Mg–N dative bond. The Mg–N interaction is less pronounced in the solvated derivatives, but the Mg–N distances in these complexes are still well below the sum of van der Waals radii of magnesium and nitrogen. Variable-temperature NMR studies showed that the transannular Mg–N interaction observed in the solid-state form is maintained in solution. This Mg–N cross-ring interaction in both the solvated and unsolvated organomagnesium *bamam* complexes results in the pronounced folding of the six-membered ring (Fig. 7).

The metrical parameters of **94** indicate localized π-bonding within the backbone of the *bamam* ligand. The folding of the six-membered ring brings the p-orbital on the central nitrogen atom in a suitable orientation to facilitate lone-pair donation to the magnesium center (Fig. 7). By contrast, the *nacnac* ligand is usually π-delocalized in metal complexes [49].

Magnesium alkoxide *nacnac* complexes have been found to be extremely active initiators for the ring-opening polymerization of *rac*-lactide (LA), however, the Mg–O bond tends to

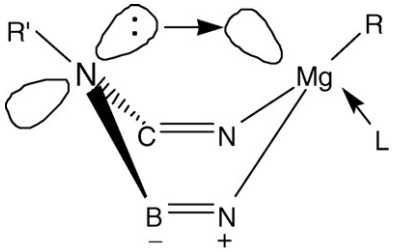

Fig. 7. Transannular interaction in **94** (the R′′ and R′′′ groups attached to the Mg-bonded N atoms have been omitted).

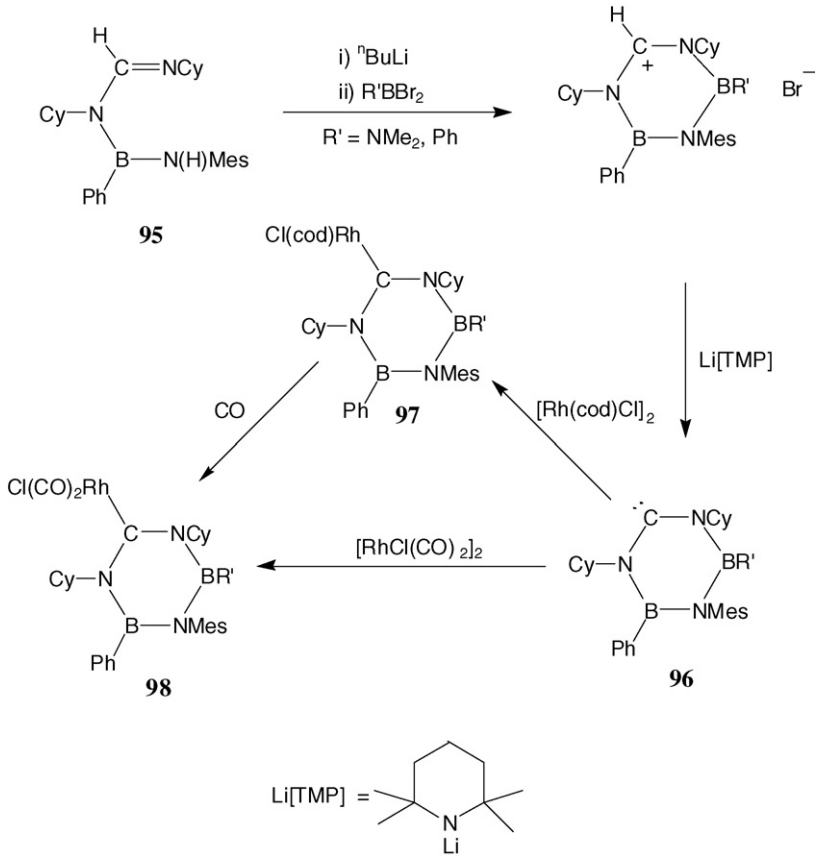

Scheme 25.

participate in unwanted side reactions thereby lowering the control of chain length of the resulting polymer [77–80]. Attempts to reduce these side reactions by lowering the Lewis acidity of the magnesium centers using a *nacnac* ligand bearing a pendant Lewis base donor group were unsuccessful [81]. In comparison, the organomagnesium *bamam* complexes inherently contain this intramolecular interaction via the transannular Mg–N contact. Preliminary studies of the polymerization of *rac*-LA by solvated Mg-*bamam* complexes have revealed that the methyl and phenyl derivatives are active initiators, whereas the *iso*-propyl and *n*-butyl derivatives are inactive [48]. However, no clear correlation between activity and the strength of this cross-ring interaction was evident.

In an interesting development of the chemistry of these hybrid ligands, Bertrand and co-workers have utilized the protio *bamam* derivative [MesN(H)](Ph)B(NCy)CH(NCy) (**95**) to make carbene analogues of borazines (**96**) (Scheme 25) [82]. The electronic properties of these novel carbenes can be readily tuned by varying the nature of boron substituents (R′). As illustrated in Scheme 25, they give rise to stable complexes with rhodium, **97** and **98**. The efficiency of these carbenes as ligands for transition-metal catalysts is under investigation.

7. Conclusions and outlook

From this overview, it can be seen that the coordination chemistry of the *bam* ligand is still in its infancy. While complexes of this dianionic ligand with lithium, group 13–16 elements and the early transition metals have been investigated quite extensively, there is a dearth of studies of, *inter alia*, derivatives of the heavy alkali metals, lanthanides or late transition metals. A perusal of the complexes that have been structurally characterized reveals that the *bam* ligand exhibits versatile behavior in coordination to metal centers; seven different bonding motifs have been identified. The dianionic charge lowers the requirement for ligands around high oxidation-state metal centers, compared to that of monoanionic *ams*. Consequently, homoleptic neutral and anionic species of the type $[ML_2]^{x-}$ ($x = 0$, 1, 2) and $[ML_3]^{2-}$ are a common feature of *bam* chemistry. A second intriguing consequence of the 2^- charge is the facile tendency for redox transformations to occur in which the $[bam]^{2-}$ dianion is oxidized to the corresponding monoanion radical $[bam]^{-\bullet}$. In some cases, notably with early main-group metals, this paramagnetic ligand can be stabilized through complexation. This feature of *bam* chemistry is likely to be encountered in future studies of new coordination complexes. It could conceivably be utilized in the design and synthesis of novel paramagnetic coordination polymers. The formation of diradicals, e.g. by one-electron oxidation of **70** or **89**, is also an intriguing possibility.

The effect of replacing the bridgehead carbon atom in the *am* ligand, by a boron center in the *bam* counterpart on the reactivity of metal centers in alkene polymerization has been accorded scant attention. The only study to date on a titanium complex showed no activity, possibly owing to a lowering of activity at

the metal site by the presence of electrophilic boron. This aspect of *bam* chemistry also deserves further investigation.

Acknowledgments

We wish to thank Prof. Dr. F. Edelmann (Universität Magdeburg, Germany) and Dr. Jari Konu (University of Calgary) for helpful comments on this manuscript. Financial support was provided by NSERC (Canada) and the University of Calgary.

References

[1] (a) J. Barker, M. Kilner, Coord. Chem. Rev. 133 (1994) 219;
(b) F.T. Edelmann, Coord. Chem. Rev. 137 (1994) 403.
[2] W.W. Schoeller, S. Grigoleit, J. Chem. Soc, Dalton Trans. (2002) 405.
[3] A.N. Chernega, R. Gómez, M.L.H. Green, J. Chem. Soc. Chem. Commun. (1993) 1415.
[4] J.C. Flores, J.C.W. Chien, M.D. Rausch, Organometallics 14 (1995) 1827.
[5] V. Volkis, M. Shmulinson, C. Averbuj, A. Lisovskii, F.T. Edelmann, M.S. Eisen, Organometallics 17 (1998) 3155.
[6] A. Littke, N. Sleiman, C. Bensimon, D.S. Richeson, G.P.A. Yap, S.J. Brown, Organometallics 17 (1998) 446.
[7] D.A. Kissounko, J.C. Fettinger, L.R. Sita, Inorg. Chim. Acta 345 (2003) 121, and references therein.
[8] Y. Zhang, E.K. Reeder, R.J. Keaton, L.R. Sita, Organometallics 23 (2004) 3512.
[9] M.J.R. Brandsma, E.A.C. Brussee, A. Meetsma, B. Hessen, J.H. Teuben, Eur. J. Inorg. Chem. (1998) 1867.
[10] E.A.C. Brussee, A. Meetsma, B. Hessen, J.H. Teuben, Chem. Commun. (2000) 497.
[11] K. Shibayama, S.W. Seidel, B.M. Novak, Macromolecules 30 (1997) 3159.
[12] Z. Li, S.T. Barry, R.G. Gordon, Inorg. Chem. 44 (2005) 1728.
[13] K.B. Aubrecht, K. Chang, M.A. Hillmyer, W.B. Tolman, J. Poly. Sci.: A 39 (2001) 284.
[14] Y. Luo, Y. Yao, Q. Shen, J. Sun, L. Weng, J. Organomet. Chem. 662 (2002) 144.
[15] C. Villiers, P. Thuéry, M. Ephritikhine, Eur. J. Inorg. Chem. (2004) 4624.
[16] R. Duchateau, A. Meetsma, J.H. Teuben, Chem. Commun. (1996) 223.
[17] M.P. Coles, R.F. Jordan, J. Am. Chem. Soc. 119 (1997) 8125.
[18] S. Dagorne, I.A. Guzei, M.P. Coles, R.F. Jordan, J. Am. Chem. Soc. 122 (2000) 274.
[19] G. Talarico, P.H.M. Budzelaar, A.W. Gal, J. Comput. Chem. 21 (2000) 398.
[20] G. Talarico, P.H.M. Budzelaar, Organometallics 19 (2000) 5691.
[21] G. Talarico, V. Busico, P.H.M. Budzelaar, Organometallics 20 (2001) 4721.
[22] R.J. Meier, E. Koglin, J. Phys. Chem. A 105 (2001) 3867.
[23] For a review that includes a brief synopsis of early work on *bam* complexes, see:
P. Blais, J.K. Brask, T. Chivers, C. Fedorchuk, G. Schatte, in: P.J. Shapiro, D.A. Atwood (Eds.), Group 13 Chemistry: From Fundamentals to Applications, ACS Symposium Series 822, 2002, p. 195.
[24] T. Chivers, D.J. Eisler, C. Fedorchuk, G. Schatte, H.M. Tuononen, R.T. Boeré, Chem. Commun. (2005) 3930.
[25] H. Fußstetter, H. Nöth, Chem. Ber. 112 (1979) 3672.
[26] D. Gudat, E. Niecke, M. Nieger, P. Paetzold, Chem. Ber. 121 (1988) 565.
[27] D. Fest, C.D. Habben, A. Meller, G.M. Sheldrick, D. Stalke, F. Pauer, Chem. Ber. 123 (1990) 703.
[28] A. Heine, D. Fest, D. Stalke, C.D. Habben, A. Meller, G.M. Sheldrick, J. Chem. Soc. Chem. Commun. (1990) 742.
[29] C.D. Habben, R. Herbst-Irmer, M. Noltemeyer, Z. Naturforsch. 46b (1991) 625.
[30] C.D. Habben, A. Heine, G.M. Sheldrick, D. Stalke, M. Bühl, P.V.R. Schleyer, Chem. Ber. 124 (1991) 47.
[31] P. Paetzold, D. Hahnfeld, U. Englert, W. Wojnowski, B. Dreczewski, Z. Pawelec, L. Walz, Chem. Ber. 125 (1992) 1073.
[32] C.D. Habben, A. Heine, G.M. Sheldrick, D. Stalke, Z. Naturforsch. 47b (1992) 1367.
[33] H.-J. Koch, H.W. Roesky, R. Bohra, M. Noltemeyer, H.-G. Schmidt, Angew. Chem. Int. Ed. Engl. 31 (1992) 598.
[34] H.-J. Koch, H.W. Roesky, S. Besser, R. Herbst-Irmer, Chem. Ber. 126 (1993) 571.
[35] M. Geschwentner, M. Noltemeyer, G. Elter, A. Meller, Z. Anorg. Allg. Chem. 620 (1994) 1403.
[36] T. Chivers, X. Gao, M. Parvez, Angew. Chem. Int. Ed. Engl. 34 (1995) 2549.
[37] W. Luthin, J.-G. Stratmann, G. Elter, A. Meller, A. Heine, H. Gornitzka, Z. Anorg. Allg. Chem. 621 (1995) 1995.
[38] T. Albrecht, G. Elter, M. Noltemeyer, A. Meller, Z. Anorg. Allg. Chem. 624 (1998) 1514.
[39] J.K. Brask, T. Chivers, G. Schatte, Chem. Commun. (2000) 1805.
[40] (a) T. Chivers, C. Fedorchuk, G. Schatte, J.K. Brask, Can. J. Chem. 80 (2002) 821;
(b) M.S. Balakrishna, J. Konu, T. Chivers, 2006, unpublished results.
[41] T. Chivers, C. Fedorchuk, M. Parvez, Inorg. Chem. 43 (2004) 2643.
[42] D.R. Manke, D.G. Nocera, Polyhedron 25 (2006) 493.
[43] D.R. Manke, D.G. Nocera, Inorg. Chem. 42 (2003) 4431.
[44] D.R. Manke, D.G. Nocera, Inorg. Chim. Acta 345 (2003) 235.
[45] D.R. Manke, Z.-H. Loh, D.G. Nocera, Inorg. Chem. 43 (2004) 3618.
[46] (a) T. Chivers, D.J. Eisler, C. Fedorchuk, G. Schatte, H.M. Tuononen, R.T. Boeré, Inorg. Chem. 45 (2006) 2119;
(b) J. Konu, M.S. Balakrishna, T. Chivers, 2006, unpublished results.
[47] T. Chivers, C. Fedorchuk, G. Schatte, M. Parvez, Inorg. Chem. 42 (2003) 2084.
[48] T. Chivers, C. Fedorchuk, M. Parvez, Organometallics 24 (2005) 580.
[49] For a review, see:
L. Bourget-Merle, M.F. Lappert, J.R. Severn, Chem. Rev. 102 (2002) 3031.
[50] B.M. Mkhailhov, T.V. Kostroma, Bull. Acad. Sci. USSR, Div. Chem. Sci. (1957) 1149.
[51] J.E. Burch, W. Gerrard, E.F. Mooney, J. Chem. Soc. (1962) 2200.
[52] U. Braun, T. Habereder, H. Nöth, H. Piotrowski, M. Warchhold, Eur. J. Inorg. Chem. (2002) 1132.
[53] J.C. Jeffery, A.P. Leedham, C.A. Russell, Polyhedron 21 (2002) 549.
[54] J.K. Brask, T. Chivers, Angew. Chem. Int. Ed. Engl. 40 (2001) 3960.
[55] G.M. Aspinall, M.C. Copsey, A.P. Leedham, C.A. Russell, Coord. Chem. Rev. 227 (2002) 217.
[56] M.C. Copsey, J.C. Jeffery, C.A. Russell, J.M. Slattery, J.A. Straughan, Chem. Commun. (2003) 2356.
[57] A. Xia, H.M. El-Kaderi, M.J. Heeg, C.H. Winter, J. Organomet. Chem. 682 (2003) 224.
[58] J.A.R. Schmidt, J. Arnold, J. Chem. Soc. Dalton Trans. (2002) 2890.
[59] A.R. Sadique, M.J. Heeg, C.H. Winter, Inorg. Chem. 40 (2001) 6349.
[60] C.-T. Chen, C.-A. Huang, Y.-R. Tzeng, B.-H. Huang, Dalton Trans. (2003) 2585.
[61] K. Kincaid, C.P. Gerlach, G.R. Giesbrecht, J.R. Hagadorn, G.D. Whitener, A. Shafir, J. Arnold, Organometallics 18 (1999) 5360.
[62] R. Duchateau, A. Meetsma, J.H. Teuben, Chem. Commun. (1996) 223.
[63] M.P. Coles, D.C. Swenson, R.F. Jordan, V.G. Young Jr., Organometallics 16 (1997) 5183.
[64] M.P. Coles, D.C. Swenson, R.F. Jordan, V.G. Young Jr., Organometallics 17 (1998) 4042.
[65] J. Barker, N.C. Blacker, P.R. Phillips, N.W. Alcock, W. Errington, M.G.H. Wallbridge, J. Chem. Soc. Dalton Trans. (1996) 431.
[66] Y. Zhou, D.S. Richeson, Inorg. Chem. 35 (1996) 2448.
[67] Y. Zhou, D.S. Richeson, Inorg. Chem. 35 (1996) 1423.
[68] D. Doyle, Y.K. Gun'ko, P.B. Hitchcock, M.F. Lappert, J. Chem. Soc. Dalton Trans. (2000) 4093.
[69] D. Abeysekera, K.N. Robertson, T.S. Cameron, J.A.C. Clyburne, Organometallics 20 (2001) 5532.
[70] T. Chivers, C. Fedorchuk, M. Parvez, Acta Cryst. C 61 (2005) o47.
[71] J.T. Patton, S.G. Feng, K.A. Abboud, Organometallics 20 (2001) 3399.
[72] H. Nöth, B. Wrackmeyer, Nuclear Magnetic Resonance Spectroscopy of Boron Compounds, Springer-Verlag, Berlin, 1978, p. 74.

[73] P. Blais, T. Chivers, A. Downard, M. Parvez, Can. J. Chem. 78 (2000) 10.
[74] N.J. Hill, J.A. Moore, M. Findlater, A.H. Cowley, Chem. Commun. (2005) 5462.
[75] M. Findlater, N.J. Hill, A.H. Cowley, Polyhedron 25 (2006) 983.
[76] N.J. Hill, M. Findlater, A.H. Cowley, Dalton Trans. (2005) 3229.
[77] B.M. Chamberlain, M. Cheng, D.R. Moore, T.M. Ovitt, E.B. Lobkovsky, G.W. Coates, J. Am. Chem. Soc. 123 (2001) 3229.
[78] M.H. Chisholm, J.C. Huffman, K. Phomphrai, J. Chem. Soc. Dalton Trans. (2001) 222.
[79] M.H. Chisholm, J. Gallucci, K. Phomphrai, Inorg. Chem. 41 (2002) 2785.
[80] M.H. Chisholm, K. Phomphrai, Inorg. Chim. Acta 350 (2003) 121.
[81] A.P. Dove, V.C. Gibson, E.L. Marshall, A.J.P. White, D.J. Williams, Dalton Trans. (2004) 570.
[82] C. Präsang, B. Donnadieu, G. Bertrand, J. Am. Chem. Soc. 127 (2005) 10182.